Brigham Young University
BYU ScholarsArchive

Theses and Dissertations

2013-12-01

Proteins in High Electric Fields

David Michael Landry
Brigham Young University - Provo

Follow this and additional works at: https://scholarsarchive.byu.edu/etd

Part of the Electrical and Computer Engineering Commons

BYU ScholarsArchive Citation

Landry, David Michael, "Proteins in High Electric Fields" (2013). *Theses and Dissertations*. 4286.
https://scholarsarchive.byu.edu/etd/4286

This Thesis is brought to you for free and open access by BYU ScholarsArchive. It has been accepted for inclusion in Theses and Dissertations by an authorized administrator of BYU ScholarsArchive. For more information, please contact scholarsarchive@byu.edu, ellen_amatangelo@byu.edu.

Proteins in High Electric Fields

David M.W. Landry

A thesis submitted to the faculty of
Brigham Young University
in partial fulfillment of the requirements for the degree of

Master of Science

Gregory P. Nordin, Chair
Brian A. Mazzeo
Stephen M. Schultz

Department of Electrical and Computer Engineering

Brigham Young University

December 2013

Copyright © 2013 David M.W. Landry

All Rights Reserved

ABSTRACT

Proteins in High Electric Fields

David M.W. Landry
Department of Electrical and Computer Engineering
Master of Science

Being able to control protein function directly and in real time is attractive. In this thesis, I discuss controlling protein activity using alternating current electric fields on the order of 1 MV/m. Since protein structures result in localized and/or protein-wide charge gradients, it is expected that a sufficiently high electric field applied across a protein should result in structural distortions which can temporarily alter or halt protein function. The field is set to oscillate above the influences of the electrochemical double layer effects (1 kHz) and below the level needed for hydrodynamic rotation of proteins (10 MHz). A device is used to pass this field across a small volume of sample while allowing the solution to still be observed. Through application of high electric fields, we are able to temporarily reduce the activity of a bioluminescent luciferase reaction. Activity is inferred by measurement of the intensity and wavelength of the light emitted by the luciferase reaction. As this process is explored further, it could lead to the ability to electrically control protein function.

Keywords: proteins, molecular biophysics, biotechnology, electric fields

ACKNOWLEDGMENTS

I would like to thank my wife for her continual support. I would also like to thank Dr. Greg Nordin for his guidance in classes and research through my undergraduate and graduate work at BYU. I am grateful to Dr. Brian Mazzeo whose collaboration has made this project possible. I thank Katy Dallon, Ben Tsai, and Danielle Lynn for help with device fabrication and testing. I would also like to thank Chad Rogers for advice on fabrication processes and chemical handling.

Table of Contents

List of Tables

List of Figures

Chapter 1

Introduction

Protein properties can be altered by changes in temperature, pH, cofactors, and other chemicals. Electric fields have the potential to alter protein properties without affecting other aspects of the reaction. This is particularly attractive for applications where other aspects of the reaction cannot be modified, such as in vivo protein reactions.

Since all proteins are made up of a subset of amino acids, all of which are composed primarily of hydrogen, carbon, nitrogen, and oxygen, protein behavior is determined more by shape than elemental composition. Therefore, altering the shape of a protein alters the properties of that protein. This paper examines the use of high electric fields to modify protein properties.

Multiple authors have reported on the effects of high electric fields on proteins in the context of other purposes, in particular for pulsed electric field (PEF) pasteurization [2, 3, 4, 5, 6, 7, 8]. With PEF pasteurization, a high electric field is passed through a sample of food. This field enlarges the pores in bacteria cell membrane, killing the cells and making the food safe for consumption [9]. This paper, however, examines how applying high electric fields nondestructively interfere with a luciferase reaction, thereby altering the amount of light produced in the reaction.

Luciferase is an oxidative enzyme that combines with a substrate to produce light. A common example of luciferase is firefly luciferase, used in conjunction with firefly luciferin by fireflies to attract mates and prey. In fireflies, aided by luciferase, luciferin combines with ATP and oxidizes, forming oxyluciferin in an excited state. Light is emitted as the electrons move from an excited state to their ground state. The energy emitted is visible as a weak glow that is red to yellow-green in color [1]. Commercially available luciferase works similarly when combined with a luciferin or luciferin-like substrate, but the substrate is engineered to emit light over a longer period of time.

The electromagnetic energy emitted by luciferase covers a couple hundred nanometer spectrum in the visible light spectrum [10]. Increasing the temperature causes an increase of brightness and shifts the center wavelength because of how temperature reactions [11]. Luciferase is a simple target to test the effect of high electric fields on proteins because of its spectral properties and because it requires no external excitation to luminesce.

In this thesis, first background information is discussed, including why it is expected that an electric field will interfere with protein function. Next, half-life and thermal properties of the particular luciferase and luciferase assay solution are examined. Finally, details of the experiment are given, including die design and fabrication decisions, experimental setup, and a discussion of the results.

Chapter 2

Background

In this chapter, I examine a simple model to give an estimate of the electric field magnitude that might distort luciferase. I then examine how much heat, to first order, the electric field is expected to generate when passing through a protein solution. Finally, I examine the light emission characteristics of luciferase.

From the calculations in this chapter, I determine that using high electrical fields to distort proteins seems reasonable to first order. However, exposing a protein solution to such high electric fields could produce significant heating. Protein function, particularly that of luciferase, is affected by temperature. As such, a heat sink with sufficient area is required to ensure that changes in protein function happen as a result of interactions with the electric field and not due to heating. Finally, it seems reasonable that luciferase should alter light emission characteristics based on distortions in secondary or tertiary structure, and that this can be used as a mechanism for reporting changes to protein shape.

2.1 Stretching Proteins

Proteins are composed of a linear chain of amino acid residues. The protein backbone is composed of a linked series of carbon, nitrogen, and oxygen atoms [12]. Residues may have a positive, negative, or neutral charge. How the charged residues are positioned creates a charge gradient. Over the entire protein, these charges and their positions can result in an overall dipole moment for the protein [13, 14]. Due to ionic species in the environment, this dipole moment vector can fluctuate [13].

Charged residues affect the conformation of the protein and its orientation with respect to other objects around it, such as cell membranes [15, 16]. As such, the location and sequence of charged residues is commonly used in predicting protein topology [17, 18].

Since proteins have dipole moments, the dipole moment can interact with an electric field. Given an electric field oscillating at the right frequency and intensity, that interaction could result in a distortion of the normal protein conformation. Fluctuations in the dipole moment due to environmental factors might result in similarly fluctuating conformation distortions. Additionally, residues can produce charge gradients that do not follow the symmetry of the protein and/or across multiple axes. When an electric field is applied, this could result in deformations that do not follow the symmetry of the protein. Since protein shape is linked to protein function, distortions in conformation are likely to affect function.

2.2 Heat Generation and Dissipation

The spectral brightness and hue of luciferase has a documented temperature dependence [11]. Using an electric field to deform proteins implies passing an electric current through the solution. As such, we must account for the generated heat.

Ions in a liquid contribute to the conductivity based on their mobility. The contribution of electrical conductivity for a given ion is $n_i z_i e \mu_i$, where n_i is the ion concentration, $z_i e$ is the charge on the ion, and μ_i is the ion mobility [19]. We can look at the total electrical conductivity as a sum of each type of ion and its respective mobility and concentration

$$\sigma = e \sum_i n_i z_i \mu_i. \tag{2.1}$$

The power dissipated as heat, P, is a function of conductivity, σ, electric field strength, E, and volume, V

$$P = E^2 V \sigma. \tag{2.2}$$

Given that the conductivity of a protein solution is fairly high and that the electric field to stretch a protein is on the order of 10^7, this implies significant heating caused by the electric field. Since the spectral properties of luciferase are temperature dependent, how well the experimental setup dissipates heat is important to discuss.

By combining Equation 2.2 with the equation for heat capacity, an expression for the rate of temperature change, $\frac{\partial \Delta T}{\partial t}$, is derived as a function of volumetric heat capacity, C_h, electric field, and conductivity,

$$Q = C_h \Delta T, \tag{2.3}$$

$$\frac{\partial Q}{\partial t} = C_h \frac{\partial \Delta T}{\partial t} = P/V, \tag{2.4}$$

$$\frac{\partial \Delta T}{\partial t} = \frac{P/V}{C_h} = \frac{E^2 \sigma}{C_h}, \tag{2.5}$$

where Q is the volumetric heat flow.

The typical heat capacity of water is 4.2 MJ/(m^3 K). Since the heat capacity term is much smaller than the squared electric field term, it is reasonable to assume that without some sort of heat sink to conduct the heat away from the luciferase, heat generation would likely be a major problem when dealing with high electric fields.

By making some assumptions about the conductivity of the protein solution and the volume through which the electric field conducts, we can get a rough estimate of the power dissipated through heat. We will assume a cylinder with a radius of 1.3 mm and a thickness of 1 µm. A reasonable conductivity might be 1.5 S/m for a 0.15 M protein solution. We will also assume the same strength electric field mentioned earlier (10^7 V/m). Given that enough current is available from the voltage source, this will result in a heating of

$$P = (10^7\,\mathrm{V/m})^2 \times \left(\pi (1.3\,\mathrm{mm})^2 (1\,\mu\mathrm{m})\right)(1.5\,\mathrm{S/m}) \tag{2.6}$$

$$= 800\,\mathrm{W}. \tag{2.7}$$

This significant heat generation is balanced out by the high thermal conductivity of water, 0.6 W/(m K) [20]. Silicon has a thermal conductivity of approximately 150 W/(m K). Aluminum has a thermal conductivity on the order of 200 W/(m K). Given enough surface area over an aluminum heat sink, the heat will quickly conduct from the water, through the silicon substrate, to the heat sink.

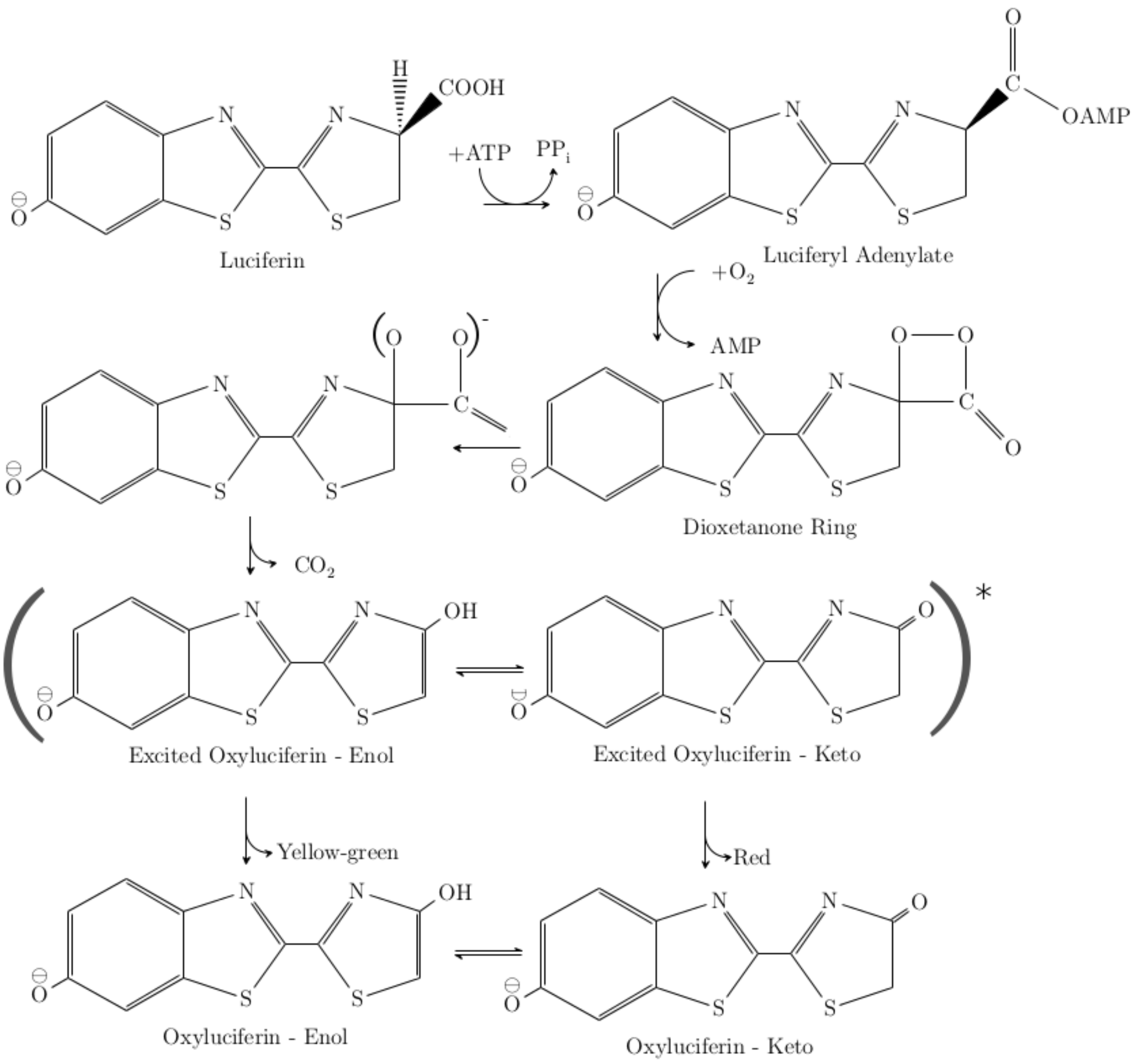

Figure 2.1: ATP activates the carboxylate group of luciferin to form luciferyl adenylate. The luciferyl adenylate combines with oxygen to create a dioxetanone ring. The dioxetanone cleaves releasing carbon dioxide and yielding oxyluciferin in an excited state. As the electrons drop to a ground state, light emits from oxyluciferin (figure based on the structure published in [1]).

2.3 Light Emission

Since stretching proteins caused by an electric field will not persist after the electric field is turned off, any measurements of the effects of the electric field must be taken while the

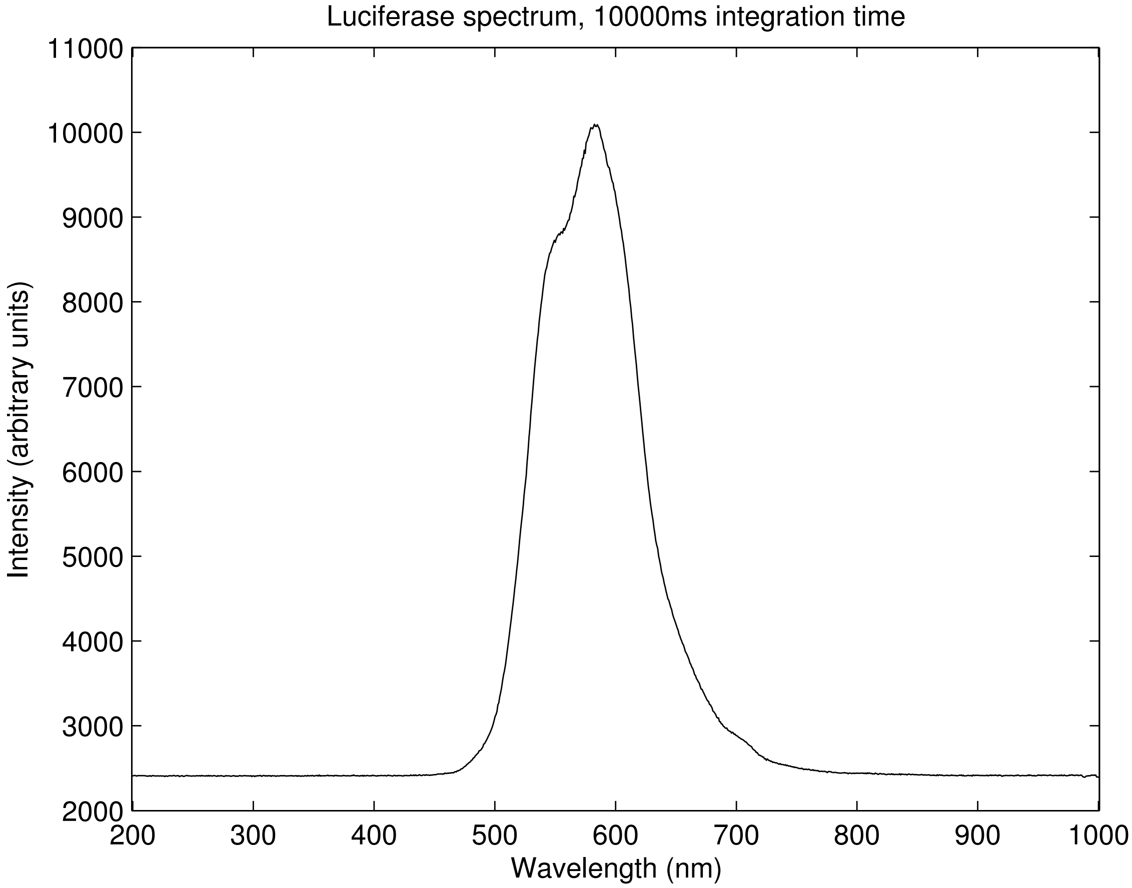

Figure 2.2: Intensity of the light emitted from luciferase as a function of wavelength recorded with an Ocean Optics QE65-ABS Spectrometer without a slit (1 mm aperture).

sample is exposed to the field. The literature suggests that measuring the emitted wavelength is a sound method for gaining insight into changes in the protein and its intermediate forms.

In 1996, Baldwin outlined the structure and light emission mechanism of firefly luciferase, pictured in Figure 2.1 [1]. As luciferin is exposed to ATP, the carboxylate group is activated, yielding luciferyl adenylate. Luciferyl adenylate combines with ambient oxygen yielding a dioxetanone ring. Dioxetanone decarboxylates to form an electronically excited state of keto or enol form oxyluciferin. As the oxyluciferin returns to the ground state, it emits visible light near ranging from yellow-green to red.

The emitted spectrum of luciferase[1] Figure 2.2 shows a peak intensity at 583 nm, with the half-power spectrum ranging from 520 nm to 636 nm. The literature shows strains of luciferase with different peak intensity wavelengths than Figure 2.2. One author reports how beetle luciferase samples elicit light with a peak ranging from 546 nm to 593 nm, concluding that the amino acid sequences of luciferases resulting in different ranges of light are 95% to 99% identical with each other [21]. It has been suggested that the tertiary structure alters the wavelength of emissions [1]. The tertiary structure of a protein encapsulates how the amino acids are ordered spatially. As such, a possible mechanism for reporting how high electric fields stretch luciferase might be to monitor this spectral shift as a high electric field is applied

It is also possible that distortions in secondary and tertiary structure could affect available reaction sites. By making some reaction sites unavailable, the electric field would slow the reaction rate and thus lower the intensity of emitted light.

Regardless of mechanism, it seems likely that a high electric field applied across a luciferase solution should affect protein activity. Changes in protein activity should be visible in the emitted light.

---

[1] The luciferase solution used is Promega's QuantiLum recombinant luciferase combined with their ONE-Glo luciferase assay system.

Chapter 3

Luciferase Characterization

Before testing how high electric fields would affect a luciferase solution, we decided it was important to characterize the solution. The specific luciferase solution used is Promega's QuantiLum recombinant luciferase mixed with their ONE-Glo luciferase assay system, a substrate containing the components necessary for the luciferase reaction (ATP, O_2, Mg^{2+}, and luciferin).

Two sets of preliminary experiments were performed to help characterize the solution. The first explored the half-life of the luciferase light output. This helped to understand how long an experiment could run in order to ensure higher protein activity. The second investigated how temperature changes affect the luciferase solution. Characterizing thermal effects is particularly important so that thermal effects and electric field effects would not be mistaken for each other.

3.1 Half-life

The luciferase reaction depends on depletable materials in the solution, such as ATP and O_2. This means the light emitted by the reaction decreases with time. This decrease in light output follows an exponential decay. To better understand how long a luciferase solution is useful, we ran tests to characterize the half-life of this luciferase enzyme.

For the experiment, we collected light with a spectrometer at an integration time of 60 seconds. The device used is the silicon die described in Sections 4.1 and 4.2. The microfluidic layer for this device was fabricated to allow for 40 µm thick cross-section of the luciferase solution. By combining this thickness with a one minute long integration time, the light output was high enough to be detectable above the noise floor for at least four or five half-lives.

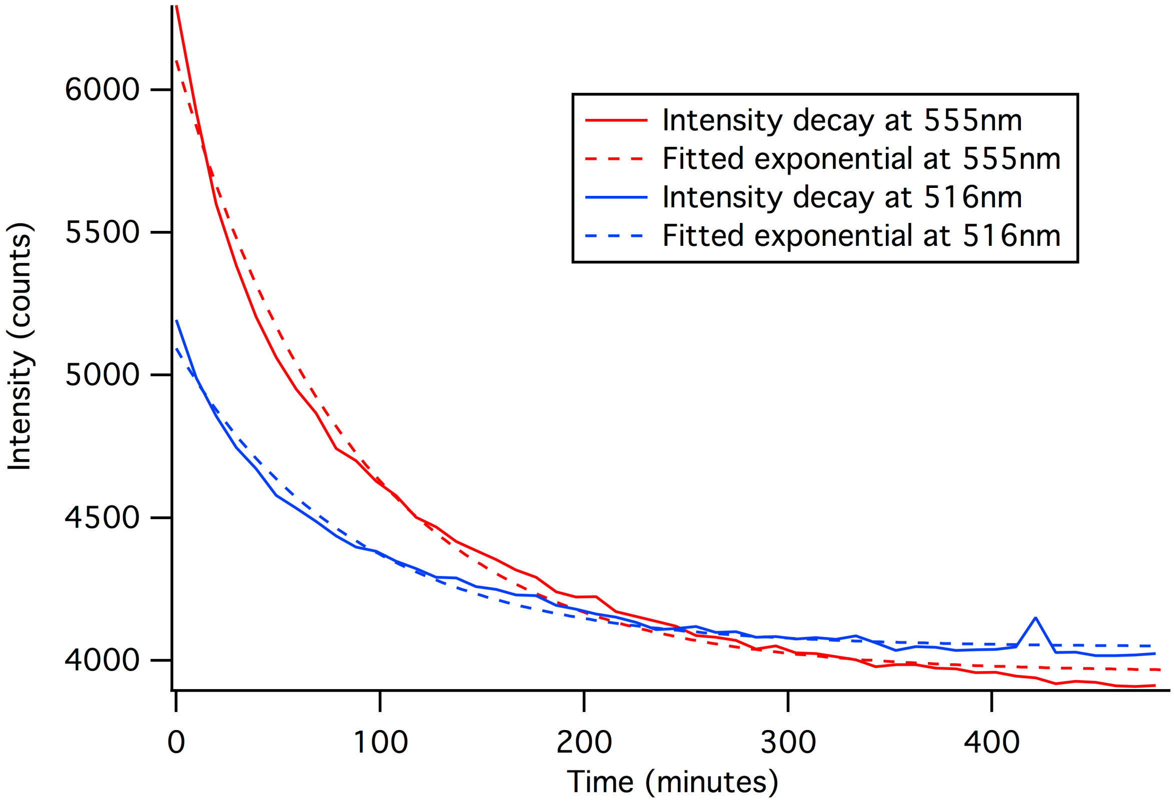

Figure 3.1: First half-life test. Results are shown as intensity vs time at two wavelengths, 555 nm and 516.56 nm. The fitted exponential for 555 nm is $3960.1 + 2143 \times e^{-0.011585t}$. Solving for the half-life gives $t_{1/2} = 59.8$ minutes. The fitted exponential is for 516.56 nm $4047.44 + 1046.8 \times e^{-0.0117388t}$. Solving for the half-life gives $t_{1/2} = 59.047$ minutes.

Light output was collected for six to eight hours. The data was then analyzed and curve fit using Igor Pro, a data analysis package by WaveMetrics, Inc. The results are shown in Figures 3.1, 3.2, and 3.3. These figures show an exponential decay in light output over time. The independent axis shows time in units of minutes. The dependent axis measures intensity in arbitrary units.

With intensity decreasing due to the normal half-life, it is expected to see a similar decay across the entire waveform. As such, multiple points were picked and the decay rate was calculated for each. The decay plot at two of these wavelengths is shown in Figures 3.1, 3.2, and 3.3. As expected, the values calculated for half-life vary by only a few minutes for different wavelengths measured during the same run. These small variations were attributed to the fact that wavelengths further from the peak wavelength reach the noise

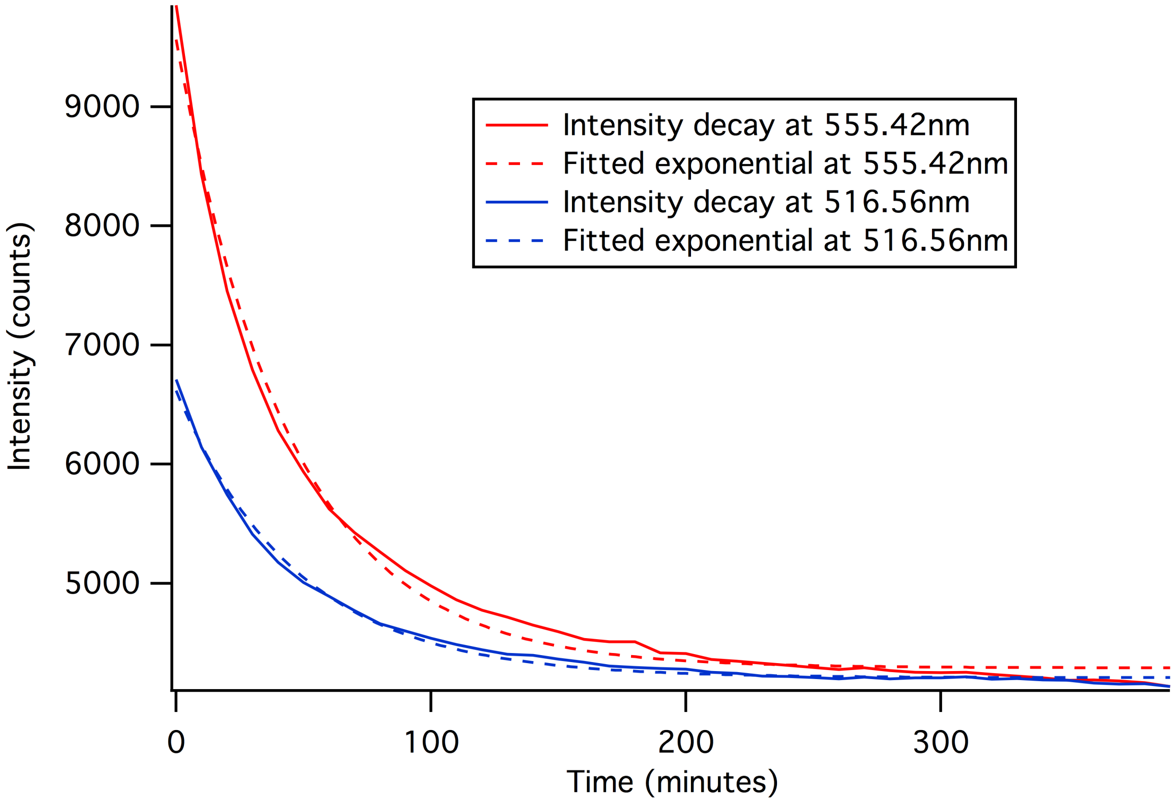

Figure 3.2: Second half-life test. Results are shown as intensity vs time at two wavelengths, 555 nm and 516.56 nm. The fitted exponential for 555 nm is $4291.71 + 5274.11 \times e^{-0.022429t}$. Solving for the half-life gives $t_{1/2} = 30.9$ minutes. The fitted exponential for 516.56 nm is $4209.17 + 2408 \times e^{-0.021044t}$. Solving for the half-life gives $t_{1/2} = 32.94$ minutes.

floor more quickly. Between runs, half-life measurements varied more, from a minimum of of 30.9 minutes in the second run (Figure 3.2) to 59 minutes in the first run (Figure 3.1). Vendor literature mentions that half-life length is affected by temperature [22]. Since each run was performed without thermal control and on different days, it seems likely that the variation in half-life was a result of variations in ambient temperature.

With this information, we were able to better plan how long we could reasonably detect luminescence. In the experiments reported in Chapter 4, it helped us to isolate changes that might have been caused by the electric field rather than normal decay.

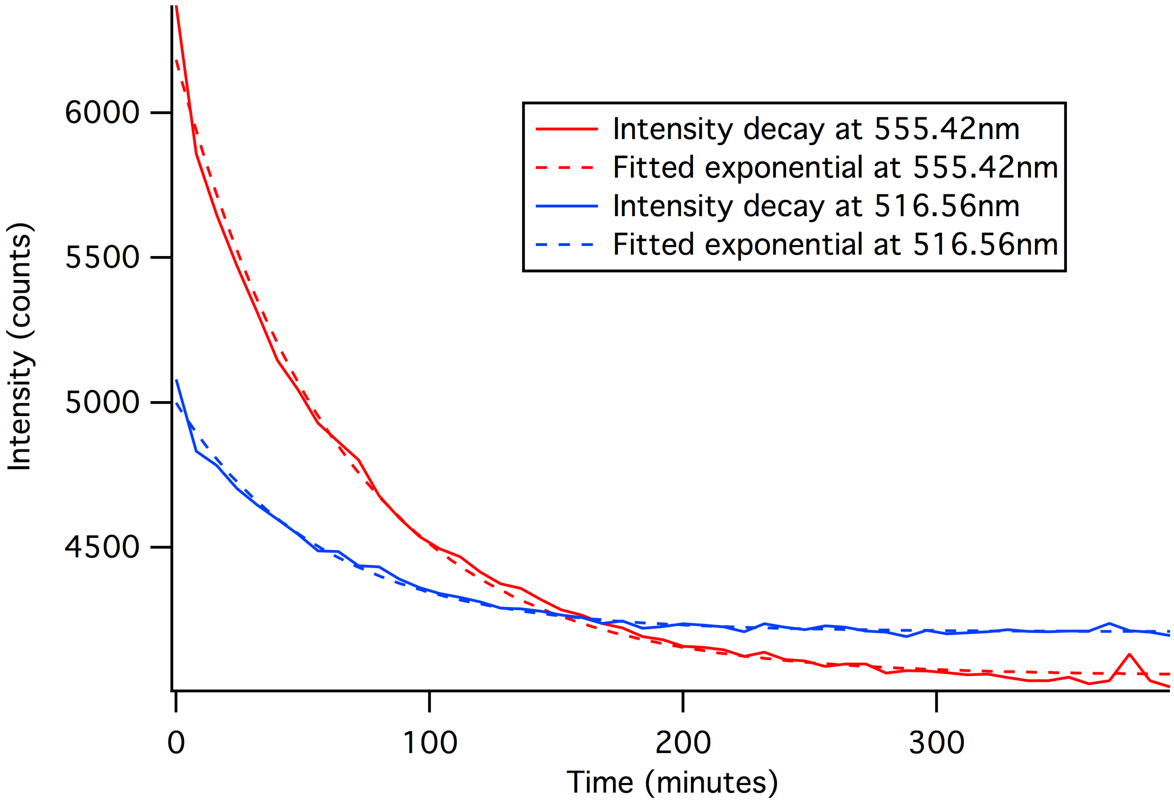

Figure 3.3: Third half-life test. Results are shown as intensity vs time at two wavelengths, 555 nm and 516.56 nm. The fitted exponential for 555 nm is $4058.34 + 2124.14 \times e^{-0.015427t}$. Solving for the half-life gives $t_{1/2} = 44.93$ minutes. The fitted exponential for 516.56 nm is $4209.6 + 790.101 \times e^{-0.0176247t}$. Solving for the half-life gives $t_{1/2} = 39.33$ minutes.

3.2 Thermal Effects

The intensity and hue of light emitted by luciferase has a documented temperature dependence [11]. While the luciferase vendor provides a rough graph depicting intensity changes with respect to temperature, they only provide three data points for this, and they provide no information about how temperature affects the color [22]. Since electric fields can produce thermal effects, it seemed prudent to properly characterize how different temperatures might affect the emitted spectrum.

Unlike the other tests outlined in this document, this test was done on bulk luciferase solutions (approximately 105 µL). The solution was poured into a thin aluminum vial which in turn was floated in a water bath. The water bath is a Thermo Scientific Neslab RTE 10 Digital Plus. It is equipped with a heater and chiller and can have its setpoint adjusted

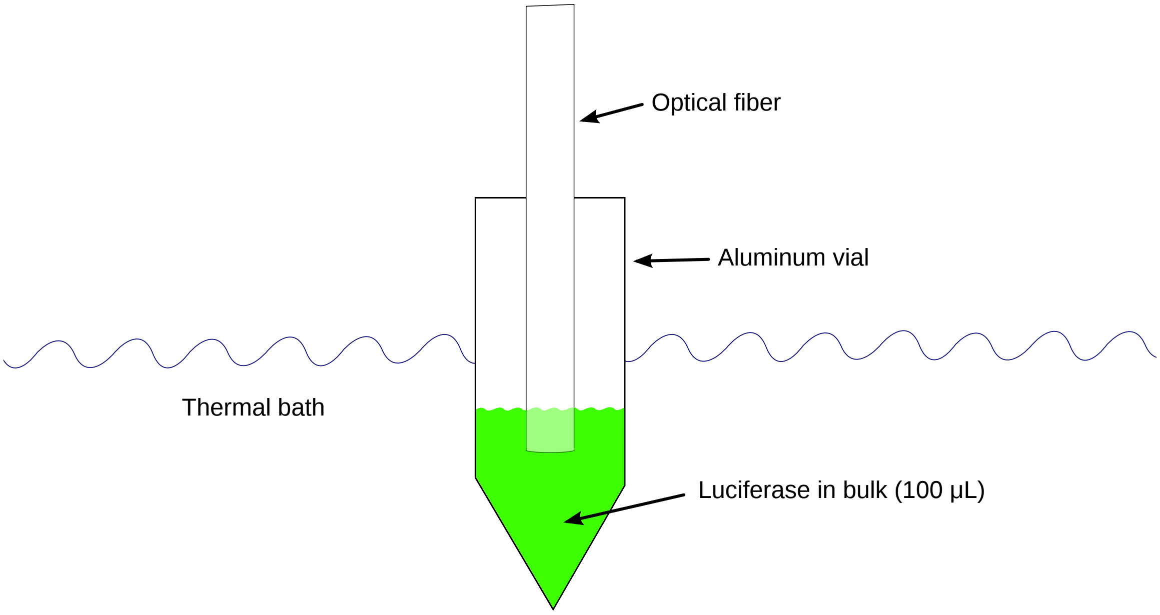

Figure 3.4: Diagram of the setup for testing thermal effects on luciferase. An aluminum vial is floated in a water bath and filled with approximately 105 µL of luciferase solution. A 1 mm core optical fiber is slightly submerged in the solution and held in place. The temperature setpoint of the water bath is ramped across a range of temperatures and the temperature and light output are recorded.

between −25 °C to 150 °C[1] in increments of 0.01 °C with ±0.01 °C stability. With the vial of luciferase floated in the bath, the fiber was then centered in the vial, centered and slightly submerged in the luciferase (see Figure 3.4 for a diagram).

In this configuration, we discovered through trial and error that the luciferase would thermally denature above 39 °C. After confirming this, further experiments were confined between 15 °C and 39 °C. While tests were performed both ramping up from 15 °C and ramping down from 39 °C, the water bath's slower cooling rate coupled with the decrease in half-life at higher temperatures made ramping down less practical. As such, the results shown in Figures 3.5, 3.6, and 3.7 are of experiments where we ramped up from 15 °C to 39 °C.

Figure 3.5 shows the expected thermal dependence of intensity. Starting at the cold end, intensity increases as temperature increases until reaching the peak temperature. As

---

[1] To operate outside of ranges where pure water remains a liquid, something other than pure water must be loaded into the bath.

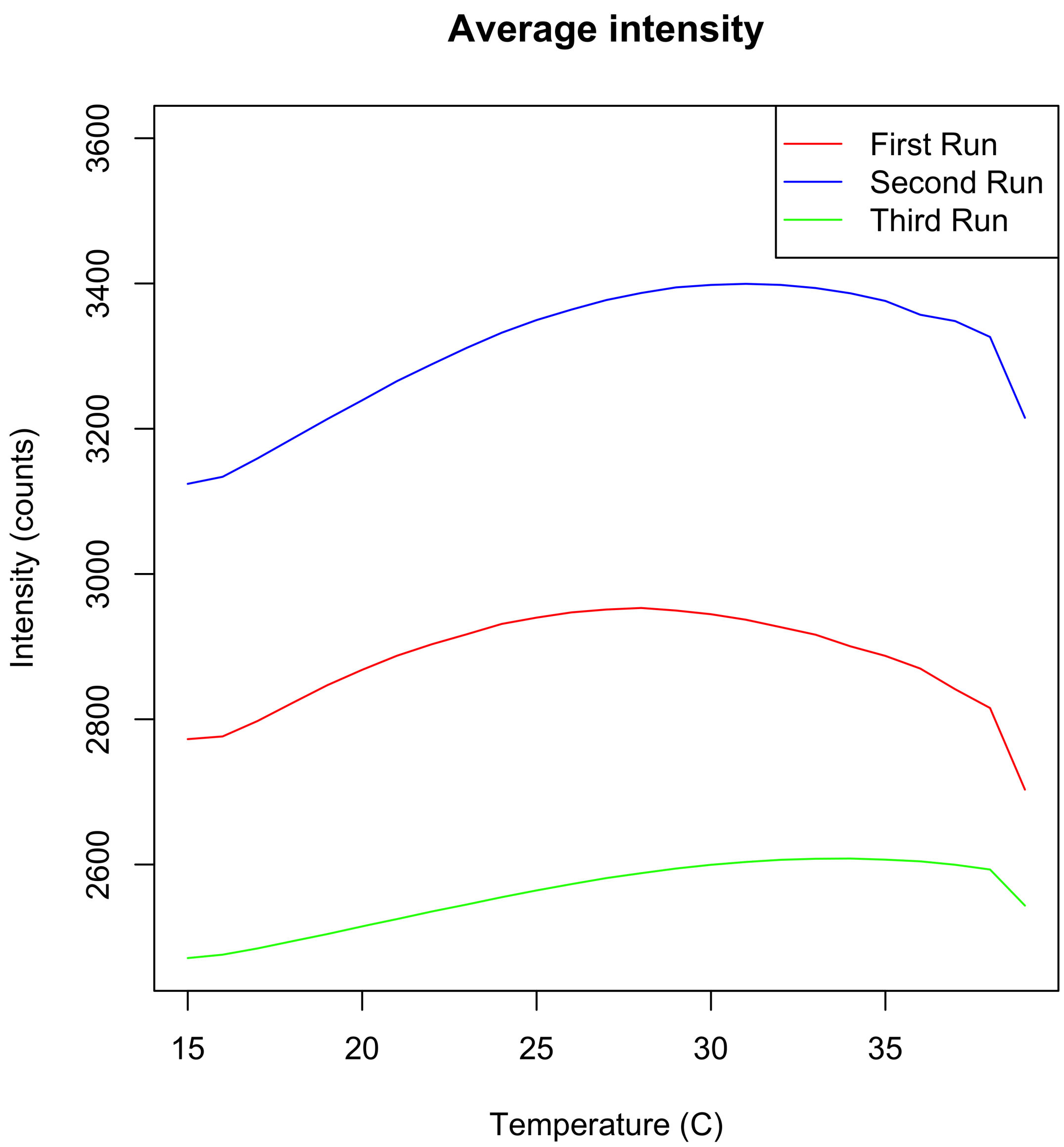

Figure 3.5: Average intensity is shown as a function of temperature for three runs. This graph shows the temperature dependence of light intensity. Intensity increases with increasing temperature until reaching the peak temperature. After this, intensity slowly drops as temperature increases.

temperature rises past the peak temperature, intensity decreases. It is important to note that the peak temperature shown in this graph does not match the peak temperature from vendor literature [22]. This seems to be caused by the thermal mass of the solution, which is likely

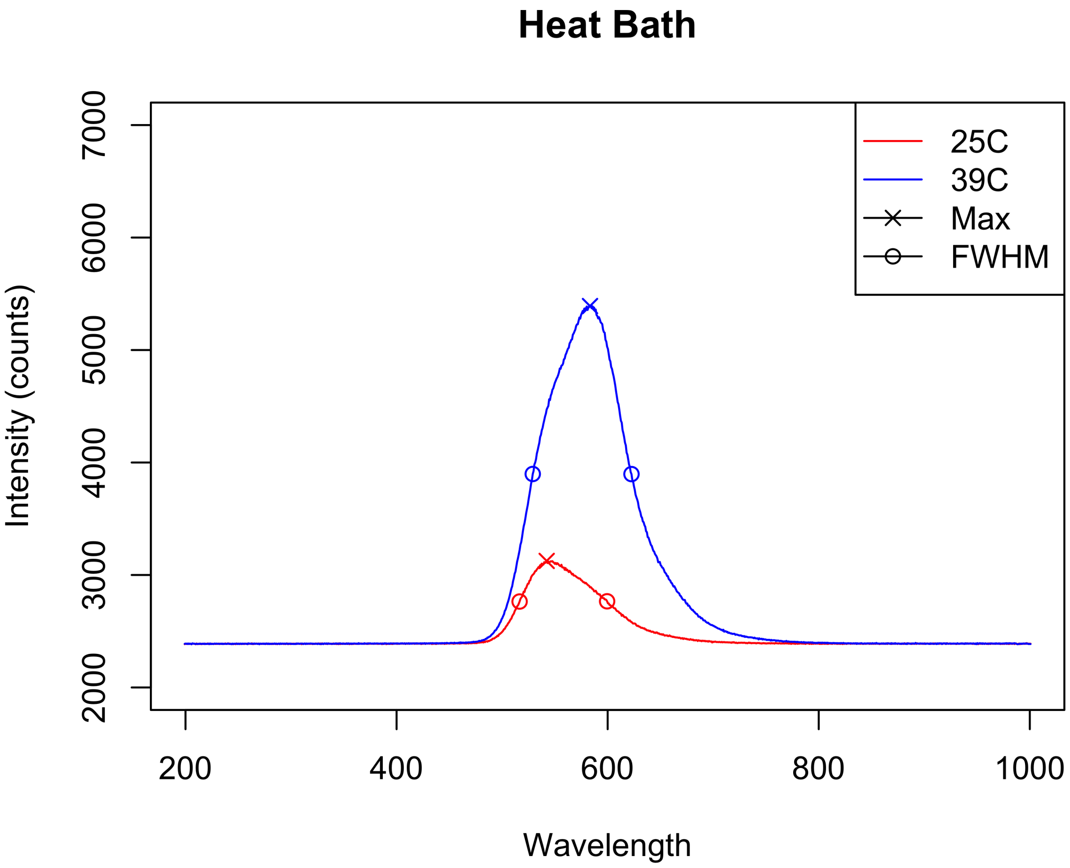

Figure 3.6: Graph of luciferase emission spectra at 25 °C and 39 °C. The peak and FWHM wavelengths have shifted as the luciferase was heated from 25 °C to 39 °C. The peak wavelength shifted 41 nm. The FWHM on the left side shifted 12.5 nm while the right side shifted 23.1 nm.

why the vendor only provides comparative data for three temperature points. Regardless, the parabolic trend in the intensity matches the trend shown in vendor data.

As the solution temperature increases, there is a shift in peak and FWHM wavelengths. Figure 3.6 shows two luciferase emission spectra at 25 °C and 39 °C. As the temperature increases from 25 °C to 39 °C, the peak wavelength increases by 41 nm. The left and right FWHM increase 12.5 nm and 23.1 nm respectively. This spectral shift is consistent across the thermal tests that were run. On average, the peak wavelength shifts around 30 nm or 40 nm.

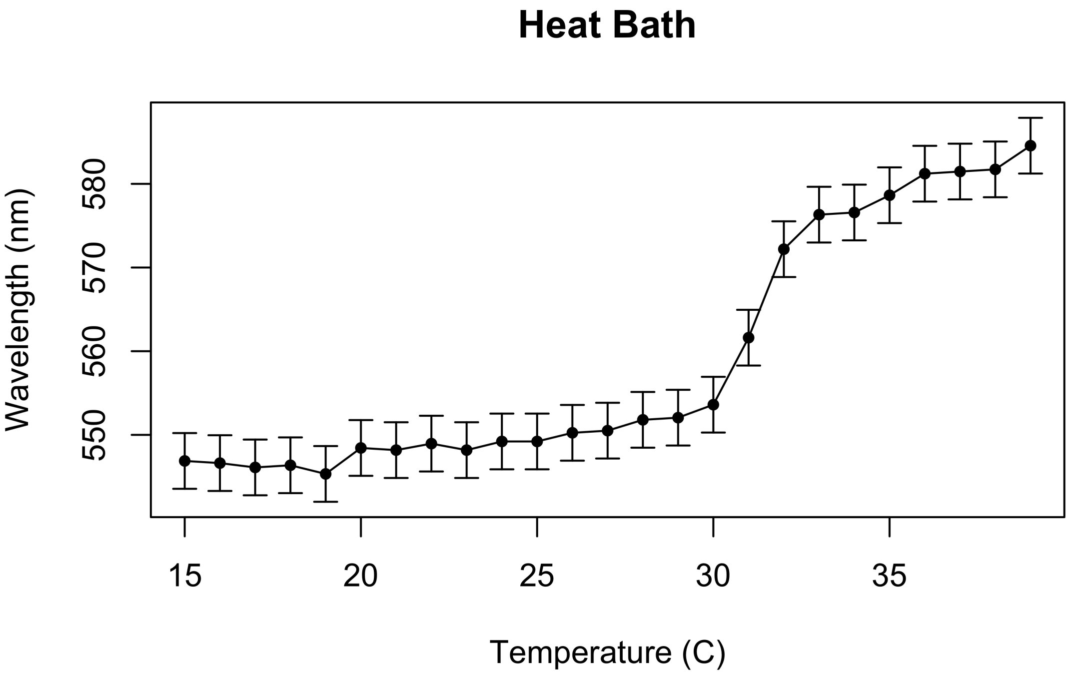

Figure 3.7: Peak wavelength as a function of temperature. Data is taken from the three runs shown in Figure 3.5. This graph shows an inflection point near 30 °C. Below 30 °C, peak wavelength gradually increases with temperature. Near 30 °C, the peak wavelength shifts dramatically. This suggests that thermal effects may be discriminated from electric field effects by watching for a shift in peak wavelength.

To characterize at what temperatures the spectrum shifts, we plotted peak wavelength as a function of temperature. Figure 3.7 shows the results. Peak wavelength generally increases with temperature. An inflection point exists near 30 °C, causing the wavelength to jump over 30 nm over a few degrees.

This consistent spectral shift gives a good mechanism for recognizing heating in luciferase. From room temperature, as little as a 10 °C increase in temperature results in a dramatic shift in wavelength.

Chapter 4

Experiment

In this chapter, I outline design consideration for the device used to test high electric field effects on luciferase. I then discuss fabrication procedures. Following is a discussion of the experiment design. Finally, results from the tested devices are presented and discussed.

4.1 Die Design

The device designed is a simple, two-layer die with an ITO-coated glass cover slip bonded on top. The first layer consists of three electrodes and traces to connect the electrodes to the voltage supply. Each electrode, when coupled with the ITO above it, creates a site for applying an electric field to luciferase. In order to maximize light collection, the electrode is designed to be larger than the fiber which collects light. The fiber used to collect light has a 1 mm diameter core and is 1.3 mm in diameter with cladding. It has a numerical aperture of 0.22, or 12.7° (about 25° full angle) acceptance angle. To ensure that the light is collected only from luciferase over the electrode, we designed the electrode to be a circle 1.3 mm in diameter.

The second layer is the fluidic layer. It provides two sites for introducing or removing fluid. These sites are connected by a channel. The channel is slightly larger than the electrodes. The fabrication techniques discussed in the next section provide a channel for the luciferase that has a cross-section of 1.5 mm by 20 µm. Because of the size of the channel, capillary action draws solution introduced in either inlet through the channel and over the electrodes. Once the fluid is pulled over the electrodes, we can test various strengths of electric fields and collect light through the ITO-coated glass cover slip.

Figure 4.1 shows the mask design used to implement the above design considerations. A blue outline shows where the die is diced. A green outline shows where the ITO-coated glass

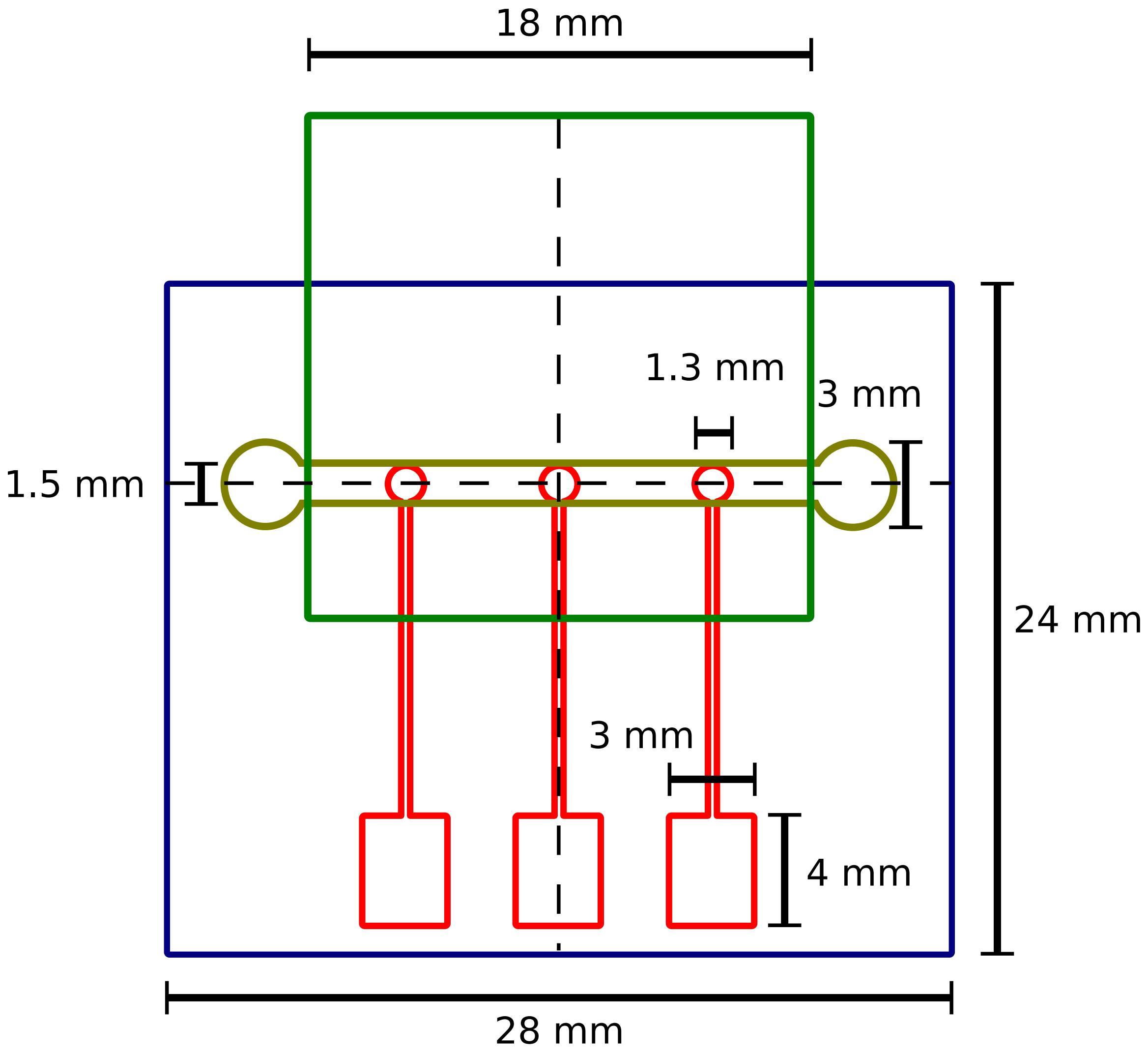

Figure 4.1: Design for the luciferase die. This image outlines the aluminum electrodes in red. The fluidic channel is outlined in dark yellow. An outline of where the ITO cover slip would sit on the finished die is in green while a blue line shows the edge of the die. Dimensions are given in black. The dashed, vertical line indicates the location of the cross-sectional diagram shown in Figure 4.2. The dashed, horizontal line corresponds in the same way to Figure 4.3.

cover slip sits after the die is diced. The red outlines with hash marks denotes the aluminum electrode layer and shows where aluminum will remain after fabrication is finished. The dark yellow outlines with dots denotes the fluidic layer and represents openings in the fluid layer to allow liquid to flow. Figures 4.2 and 4.3 show cross-sectional diagrams of the areas through the electrode and through the channel.

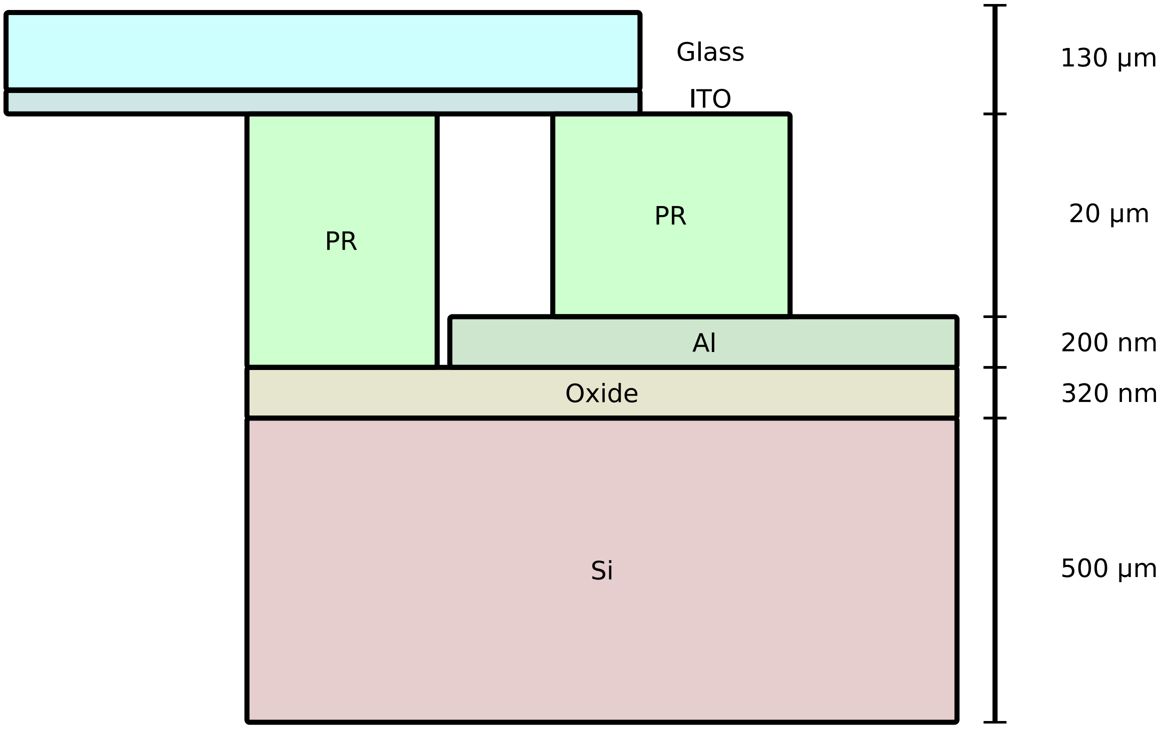

Figure 4.2: This is a cross-sectional diagram cut down the middle of an electrode It shows the layers and their thicknesses as seen down the middle of an electrode. Figure 4.1 shows a top-down view of the die. In the top-down view, the vertical dashed line indicates where this diagram cuts through the die.

4.2 Die Fabrication

The die fabrication process starts with a clean silicon wafer. A thermal oxide layer approximately 300 nm is grown to prevent conduction between the aluminum and silicon layers. A layer of aluminum is then deposited using an electron-beam or thermal evaporator. Photoresist (AZ3330) is put down and patterned with standard lithographic processes using the mask shown in Figure 4.4. Photoresist then only remains over where we want to have electrodes and metal traces. The wafer is next submerged in etchant to remove unwanted aluminum. Once all the unneeded aluminum is removed and the etchant is rinsed off, the photoresist is no longer needed and is removed. Figure 4.6 outlines this process graphically.

After patterning electrodes on the wafer, the wafer is diced into eight dies. The remaining fabrication is done using die-level processes.

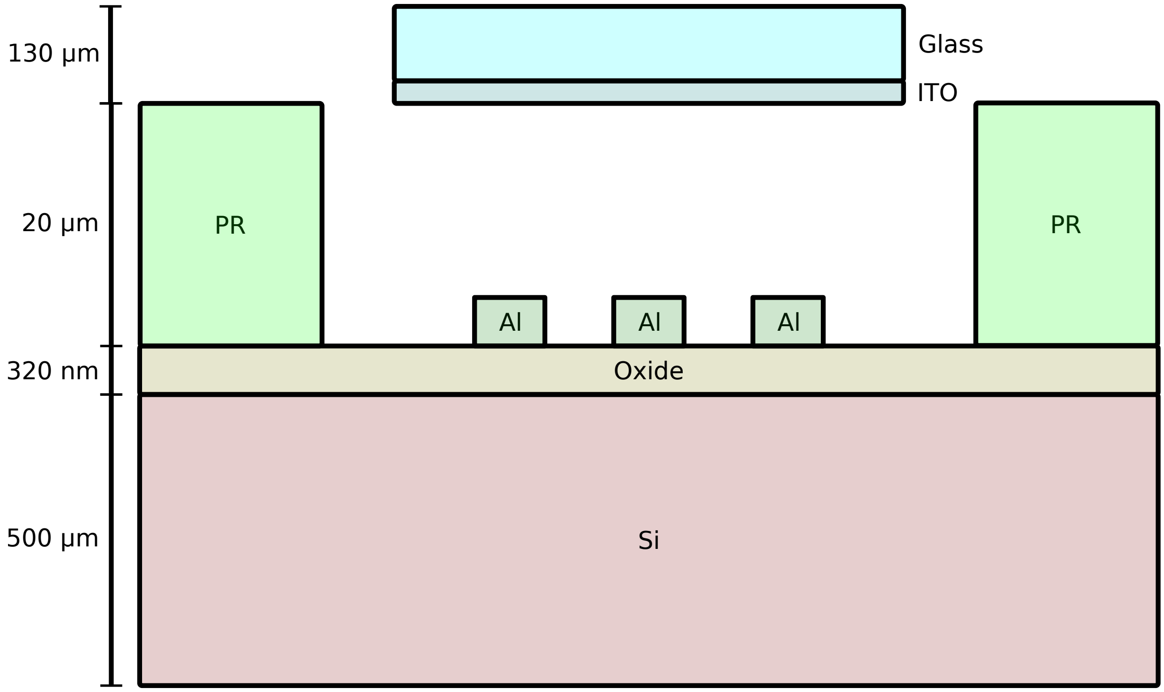

Figure 4.3: This is a cross-sectional diagram cut down the length of the channel. It shows the layers and their thicknesses as seen in the middle of the fluidic channel. Figure 4.1 shows a top-down view of the die. In the top-down view, the horizontal dashed line indicates where this diagram cuts through the die.

Fluidic layers are composed entirely of SU8-2025 (photoresist). As such, they are simple, relatively quick to fabricate, and produce a repeatable thickness. Devices have been fabricated reliably with 20 μm and 40 μm thick fluidic channels. Since a 20 μm thick channel allows us to reach electric fields twice as strong as a 40 μm channel using the same voltage, 20 μm devices were ultimately used for the experiments outlined later in this chapter.

SU8-2025 is spun onto a die. A lithographic process is used to pattern the design from Figure 4.5 onto the die. Once the pattern is transferred to the photoresist, the fluidic layer is complete. A diagram of this process is shown in Figure 4.7.

In order to bond the ITO-coated cover slip to the die, we developed a process based on the principle of photoresist reflow. When photoresist is heated, it plasticizes. In this plasticized state, surface tension reshapes the structure, rounding edges and corners. Other groups have applied this in fabricating rounded waveguides and microlenses [23, 24].

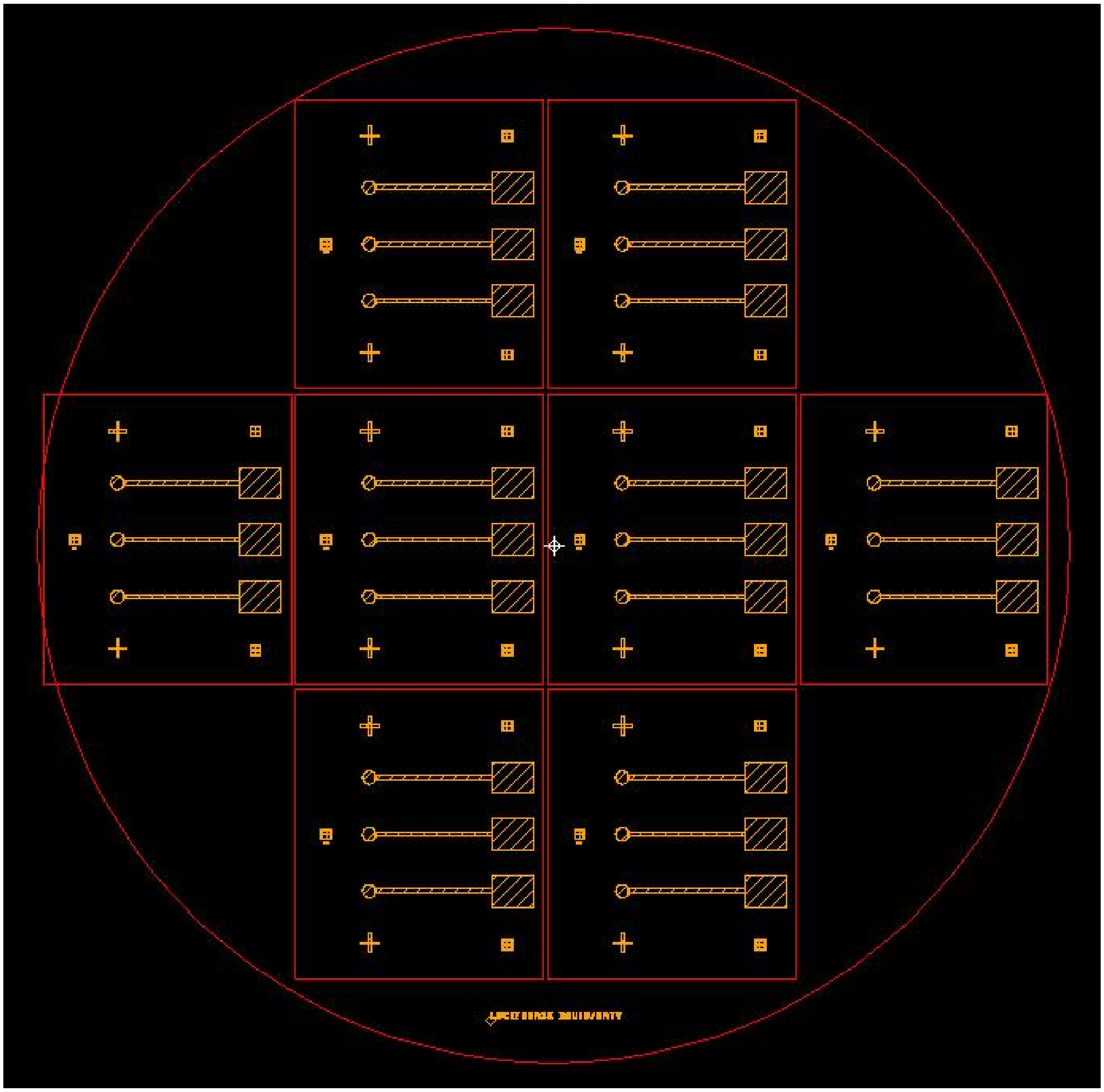

Figure 4.4: Wafer-level mask design for the aluminum layer. This image shows the metal layer from Figure 4.1 replicated eight times to maximize usage of a silicon wafer. Filled-in areas represent where aluminum remains after etching to form electrodes and traces connecting to electrodes.

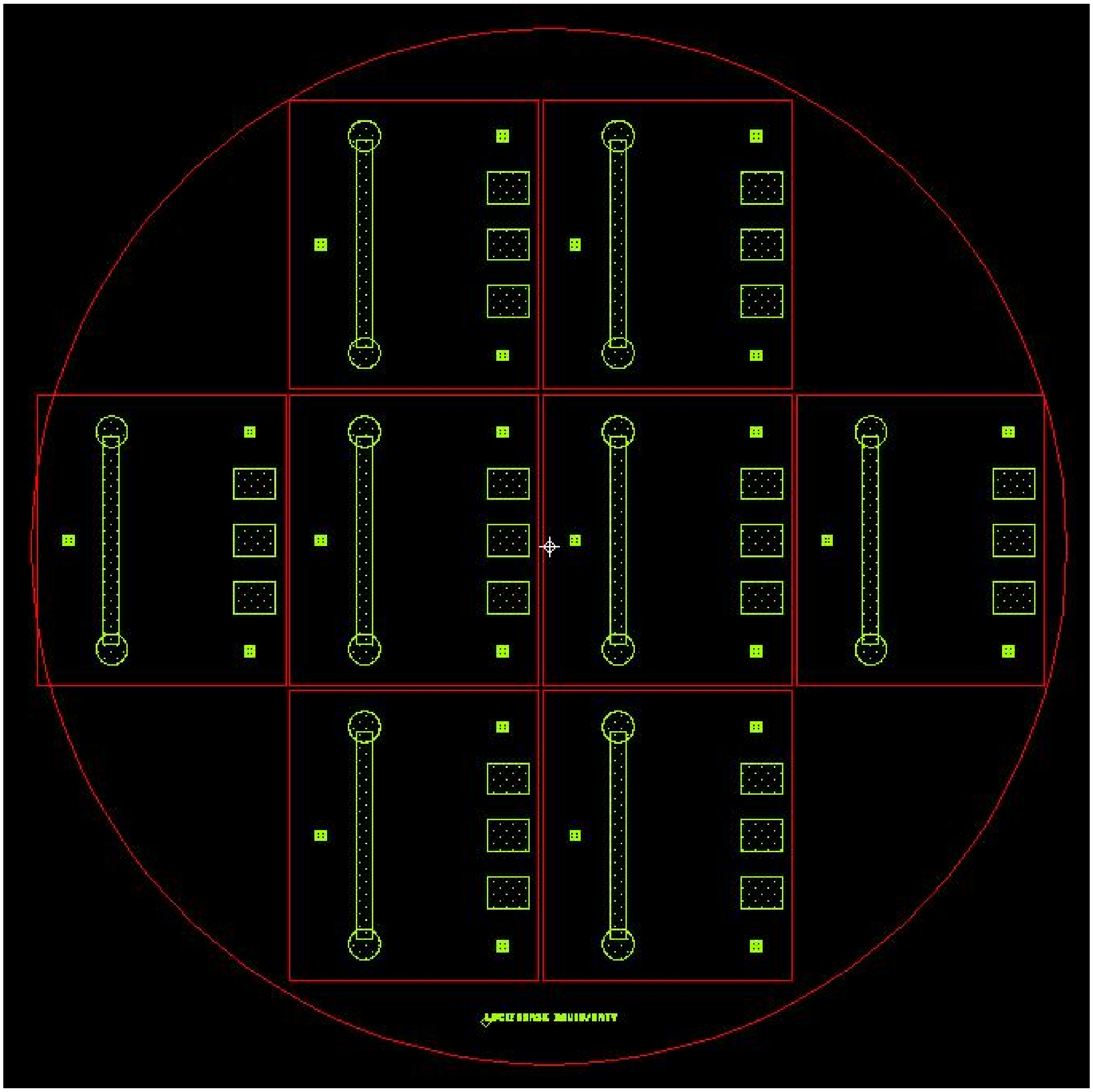

Figure 4.5: Wafer-level mask design for the fluidic layer. This image shows the fluidic layer from Figure 4.1 replicated eight times to maximize usage of a silicon wafer. Filled in areas represent where photoresist will be removed to form fluidic channels.

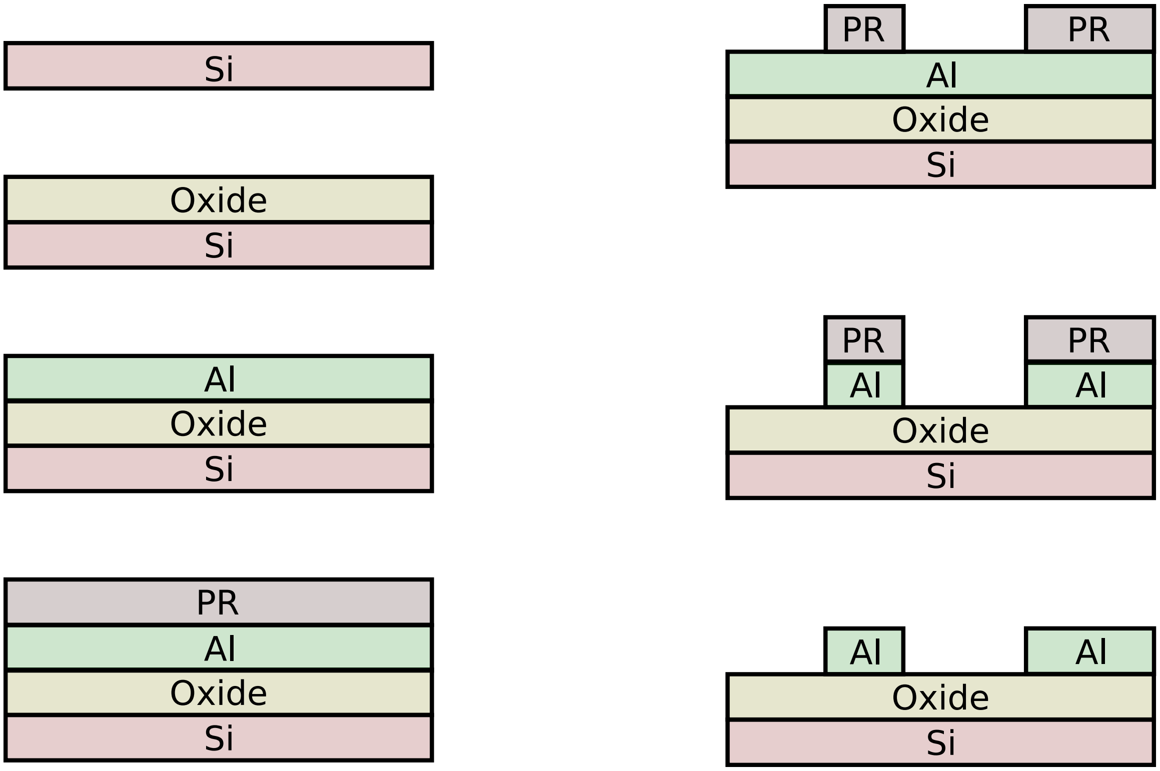

Figure 4.6: Diagram of the process to fabricate the electrodes.

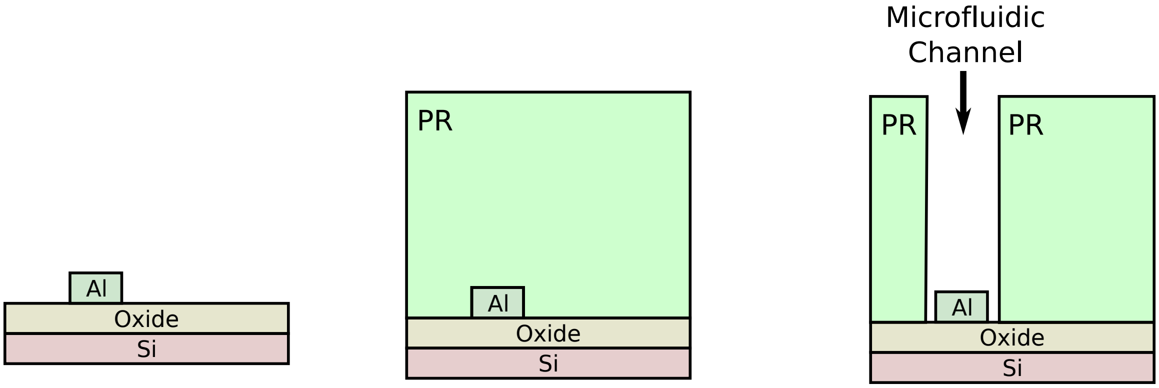

Figure 4.7: Diagram of the process to fabricate the fluidic channel.

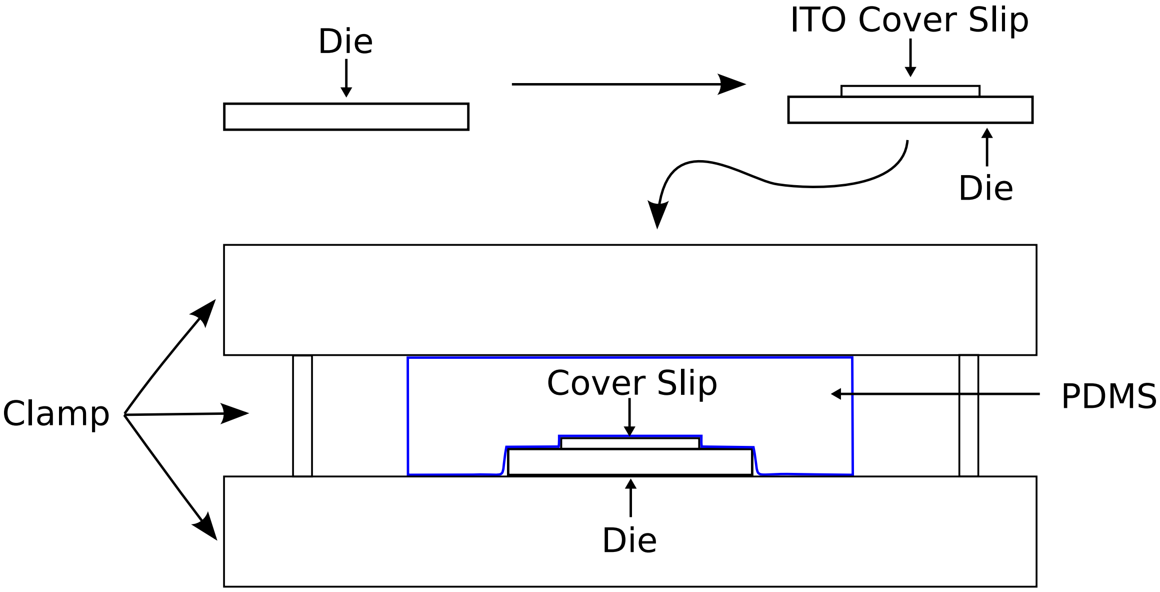

Figure 4.8: Diagram showing how ITO is bonded to the fabricated die. The cover slip and the die are pressed firmly together using a clamp. A piece of PDMS is placed between the cover slip and the clamp to help prevent the glass from breaking. The PDMS also helps distribute the pressure more evenly across the die, ensuring a consistent bond across the device.

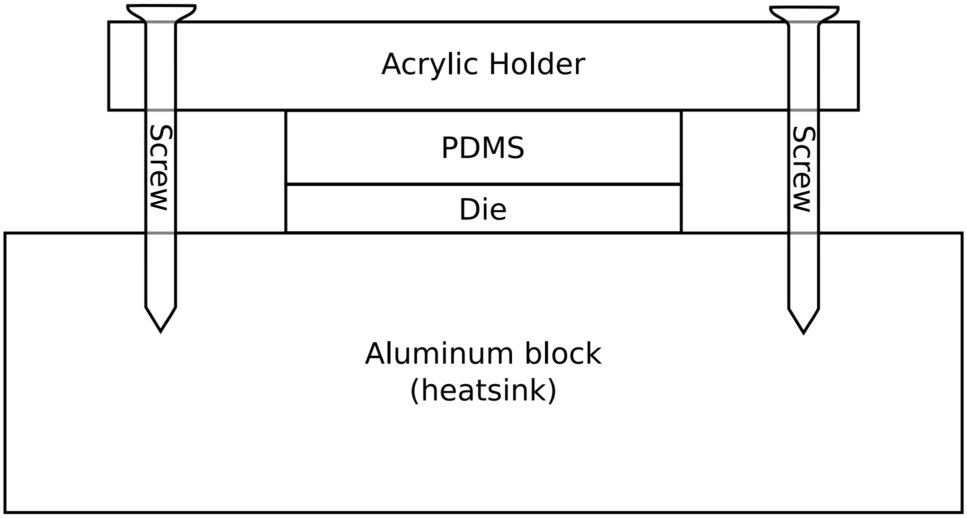

Figure 4.9: This diagram shows how the die is held in place for testing. A piece of PDMS lays over top of the die to help seal the edges of the channel. To seal the PDMS to the die, an acrylic holder presses firmly against the PDMS, held in place by two screws. The screws pull against the aluminum block which the die is resting on. The aluminum block doubles as a water-cooled heat sink to ensure that the luciferase solution stays at 22 °C. In order to water-cool the heat sink, two holes were drilled laterally through the block. These drilled holes were connected using pipe fittings and plastic hosing to the water bath described in Section 3.2.

adheres to the cover slip. After cooling and being removed from the clamp, this adhesion forms a watertight seal, creating a channel through which luciferase can flow.

4.3 Experimental Setup

To help create repeatable experimental results, we built a test fixture to hold the device. Figure 4.9 shows a diagram of the test fixture. The die sits on top of an aluminum block. This aluminum piece doubles as a water cooled heat sink. Two holes were drilled laterally through the block. Pipe fittings and plastic tubing connect these holes to the water bath mentioned Section 3.2. This setup allows us to maintain the temperature of the luciferase solution at 22 °C.

Additionally, the entire test harness is housed in a humidity chamber. It is not uncommon for the ambient relative humidity in the laboratory to be under 30%. To ensure the sample does not dry out, testing is done inside a humidity chamber where the relative humidity is maintained at 70% to 80%.

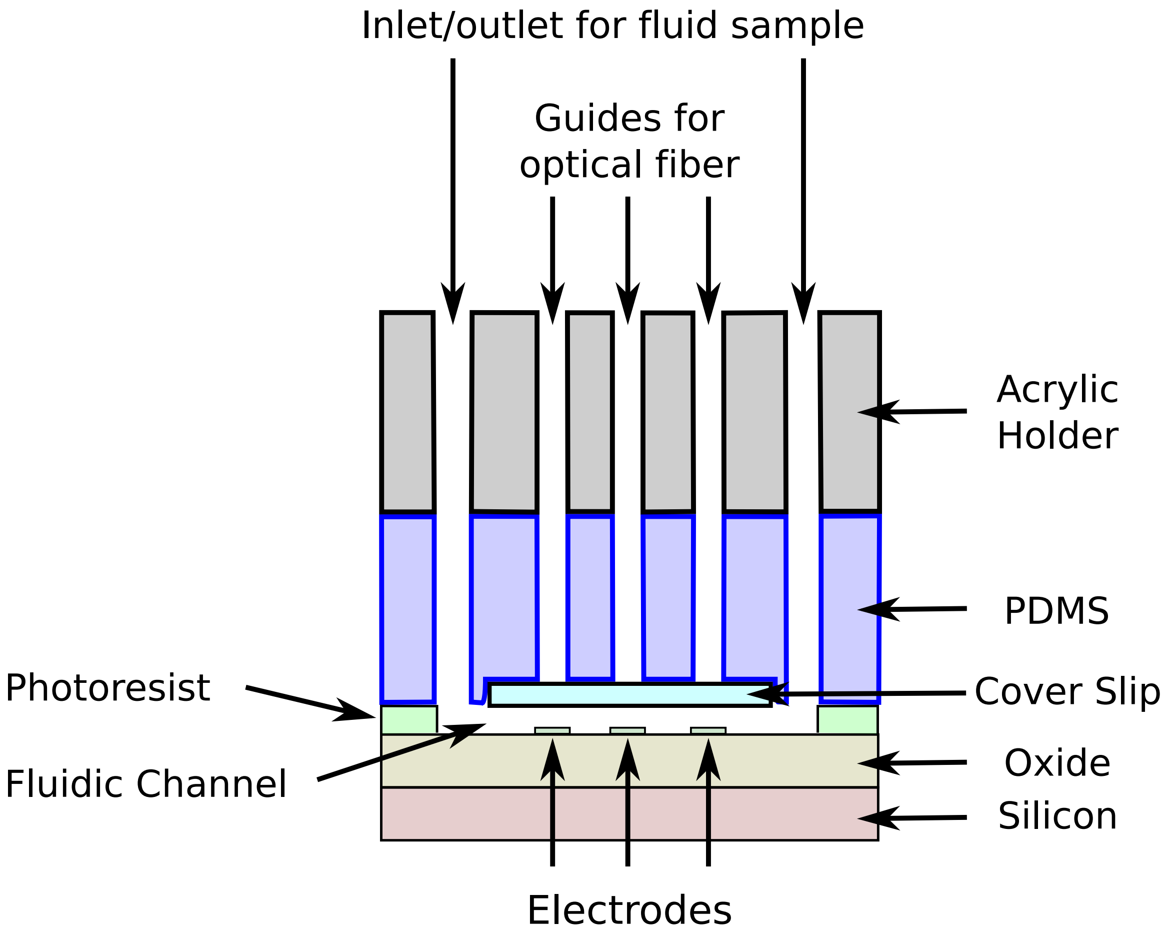

Figure 4.10: This diagram shows a longitudinal cross-sectional view of Figure 4.9 centered on the fluidic channel. In particular, this demonstrates how PDMS helps seal the inlets and outlets of the channel, allowing fluid to be more easily introduced. It also illustrates holes in the acrylic holder and PDMS which help align the optical fiber over the electrodes.

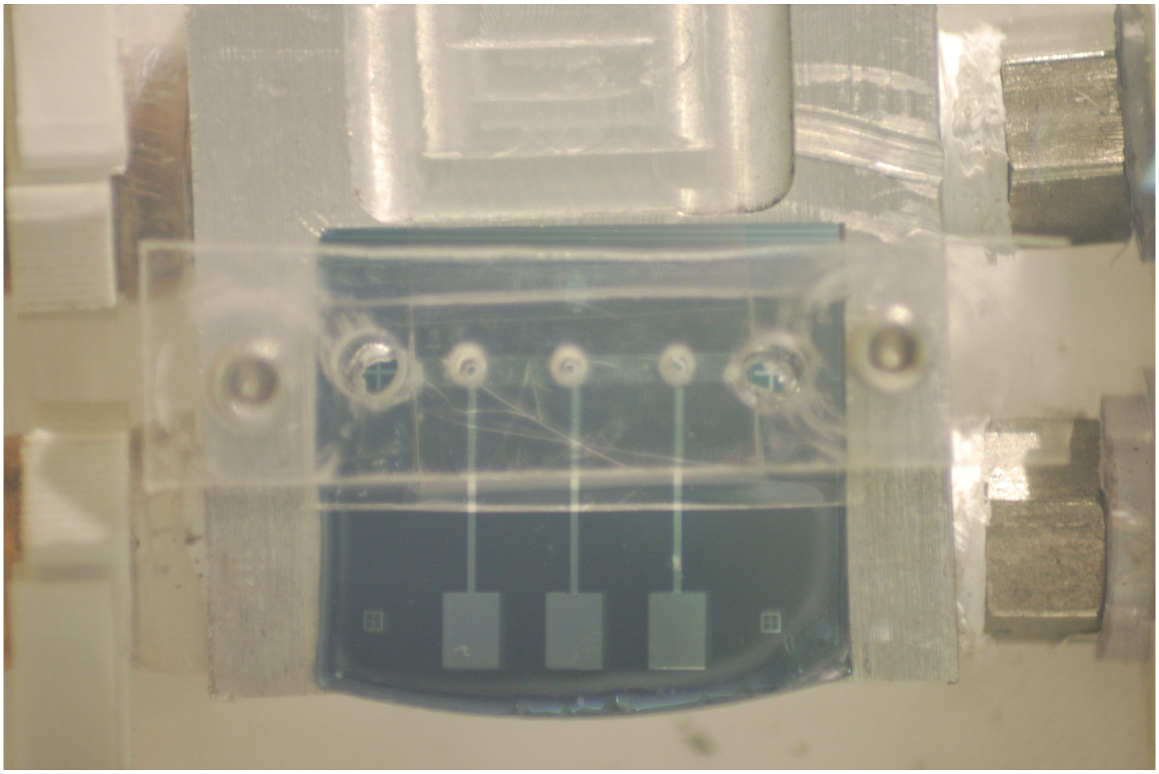

Figure 4.11: This photo shows the device in its test harness. From closer to the viewer to further away is the acrylic top piece, PDMS, die, and aluminum block. The block is connected to a water bath by four connectors, two on the left and two on the right. Water conditioned to 22 °C constantly flows through these connectors and the die to maintain the temperature of the aluminum block.

Above the die, a clear piece of PDMS is used to seal the fluidic layer's inlets to prevent solution from flowing over the top of the cover slip. A clear piece of acrylic sits on top of the PDMS. The acrylic is pressed towards the die using screws or bolts screwed into the aluminum block. Pushing the acrylic against the die seals the PDMS against the die. This setup allows us to keep the solution in the channel and at a consistent temperature.

It is also important to account for how light would be collected from the device and how fluid would be introduced into the device. Figure 4.10 demonstrates how these problems were solved. It shows a cross-section through the device and test harness cut longitudinally along the fluidic channel.

To allow fluid to be introduced into the device, the acrylic and PDMS pieces have two holes drilled, exposing the device's inlet. The pressure of the PDMS against the die, coupled with capillary action, helps guide solution down through the channel.

Above each electrode, a smaller hole is drilled through the acrylic and PDMS layers. These holes are approximately 1.3 mm, the width of the optical fiber used to guide light to the spectrometer. Having such a close fit gives the added benefit of aligning the fiber over the electrode. As long as the holes in the acrylic and PDMS are lined up correctly over the electrodes, when the fiber is threaded through the holes to butt up against the ITO cover slip, it will point directly at the electrode.

Figure 4.11 shows a photo of a die in the test harness. Missing from this image are the clips connecting the device's electrodes to the function generator. Screws on the far left and right of the acrylic piece press the PDMS against the die to seal the solution in the channel. Moving toward the center of the photo, two large holes allow liquid to be introduced from either side. Three small holes above the three electrodes provide three points to test per die. Four fittings in the left and right corners show where the aluminum block connects to the water bath.

After a die is loaded into the test harness, the luciferase and luciferase assay system are removed from the freezer and thawed at room temperature. The assay system is ONE-Glo, sold by Promega, which consists of a luciferase substrate and a buffer. The luciferase is a 1.437 mg/mL luciferase solution in a 1X Phosphate-buffered saline with 1 mg/mL bovin serum albumin. Mixing 5 µL of the luciferase with 100 µL of the assay system produces the bioluminescent reaction. The luminescent solution is then introduced into the inlet using a micropipette. Inserting 15 µL to 20 µL of the luminescent solution is usually more than sufficient.

Figure 4.12 shows a photo from the same perspective as Figure 4.11. In this photo, luciferase solution has been introduced into one of the inlets and the lights have been turned off. The bright green circle on the left shows where the solution was introduced into the chip. Looking closely at the other inlet shows that it is glowing a very faint green. Since no solution was introduced into the right inlet, this indicates that capillary action has drawn the solution through the fluid channel to the other side of the die.

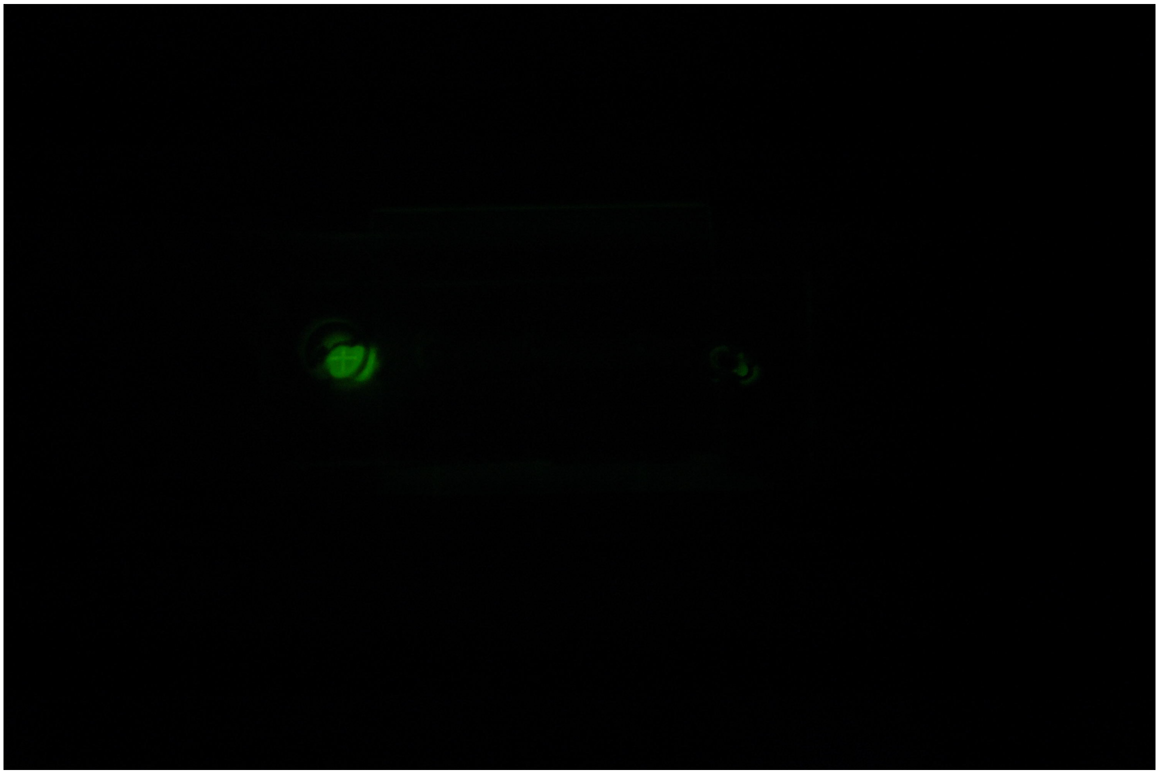

Figure 4.12: This photo was taken by the same camera and from the same position as Figure 4.11. The image was taken with a long integration time. The large green glowing circle on the left is the die's inlet filled with luciferase solution. Looking closely in a straight line to the right of this, there is a fainter green glow. This indicates that capillary action has drawn the solution through the channel to the outlet on the other side of the die.

After the die is put into the test harness, the electrical connections are made in order to enable and disable the electric field. A function generator is attached to the ITO cover slip and an electrode. Figure 4.13 shows the equivalent circuit, accounting for impedance of the solution and parasitic capacitance of the system.

Figure 4.14 shows the graph of an impedance scan of one of the devices loaded with luciferase solution. From impedance scans such as this one, we decided to operate the function generator at 100 kHz. This frequency was selected in order to operate just above the region dominated by the double layer capacitance. In the tests run so far, the function generator is usually set to 100 kHz with a voltage between 8 Vpp and 10 Vpp.

Finally, the optical fiber is inserted into the test harness. The optical fiber collects light and guides it to a spectrometer, the Ocean Optics QE6500. With the aperture used,

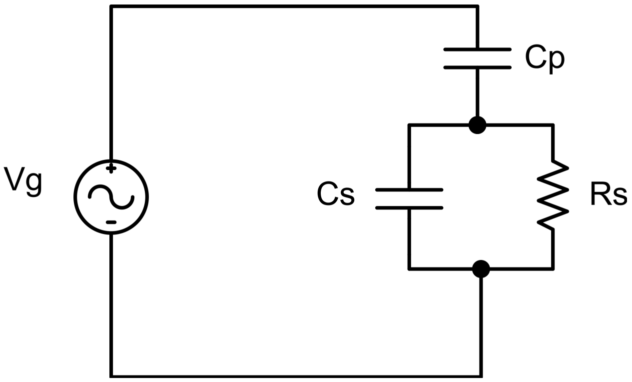

Figure 4.13: This is a schematic the equivalent circuit of the die with the function generator attached and luciferase solution introduced into the die. Parasitic capacitance is represented by **Cp**. The capacitance and resistance of the solution are represented by **Cs** and **Rs**. Finally, **Vg** is the AC voltage produced by the function generator.

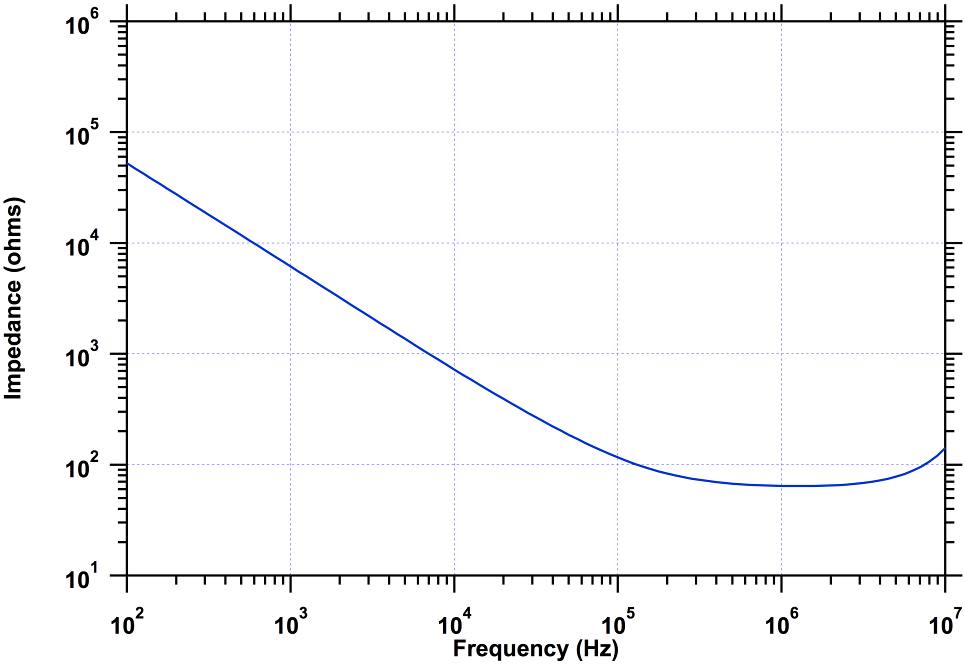

Figure 4.14: This is an impedance scan of a die loaded with luciferase solution. The scan swept from 40 Hz to 10 MHz. In this scan, the double layer capacitance region extends until approximately 100 kHz. The region where the solution is purely resistive extends from there up to a couple megahertz.

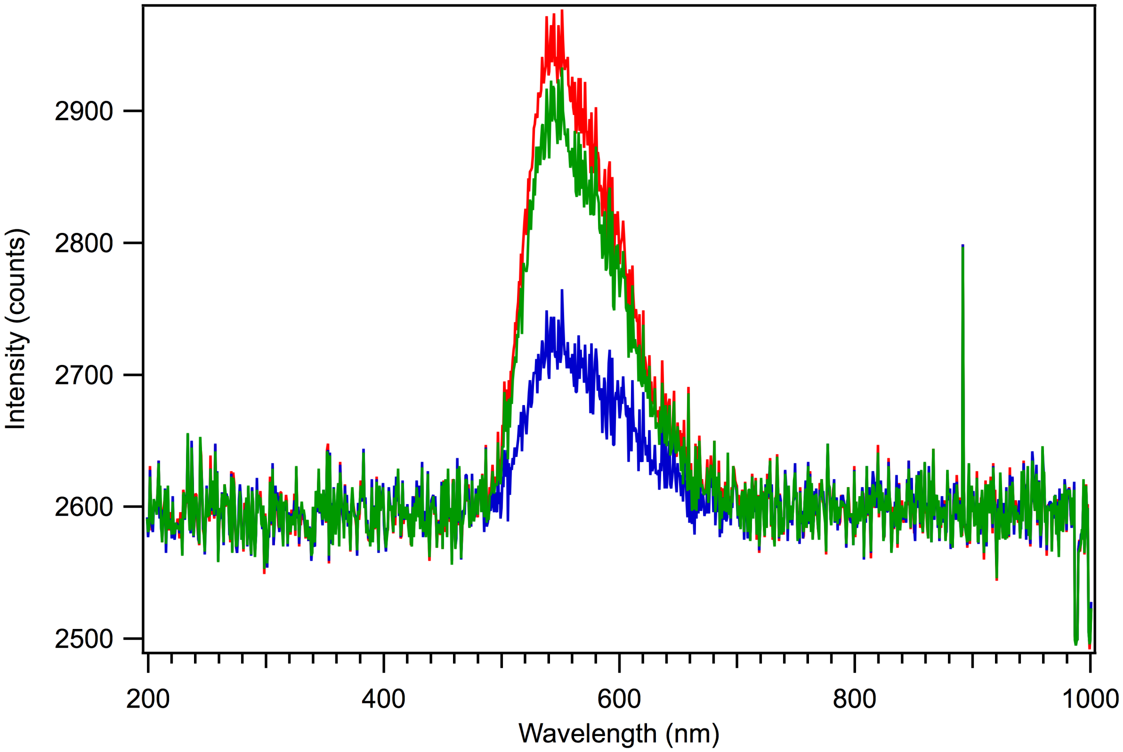

Figure 4.15: This graph shows how the wavelength of the luciferase emission does not shift when a high electric field is applied. The red line shows a spectrum taken before the electric field is applied. The blue line is a spectrum with the electric field applied. The green line is a spectrum shortly after the electric field is removed. Sample numbers in the legend correspond with the x-axis of Figure 4.17.

this spectrometer gives us a resolution of approximately 15 nm. Appendix A gives further details on the resolutions available with this device and the tradeoff between light collection and resolution.

4.4 Results

Figure 4.15 shows the spectra of three samples taken from a time series. In this series, the electric field is off, then on, then off again. The intensity of the spectrum drops noticeably when the field is enabled. When the field is disabled again, the field increases in intensity to nearly the original level. The discrepancy between the two "off" states can be attributed to the half-life of the solution.

Something of note in Figure 4.15 is that when the field is enabled, the peak wavelength does not shift. From Figures 3.6 and 3.7, we see that increasing the temperature of the luciferase solution causes a shift in wavelength, particularly the peak wavelength. Since Figure 4.15 did not show any shift in wavelength, it appears assume that some other mechanism is at work. Also notable is that the intensity decreases. Since the aluminum block is held at 22 °C, Figure 3.5 indicates that an increase in temperature in temperature should *increase* the intensity instead of the observed decrease.

In order to better observe what is happening as the electric field is applied and removed, it is helpful to look at average intensity. For the graphs of average intensity, an average is taken of the intensities between 477 nm and 709 nm for each sample[1]. After taking these averages, we are left with a time series of average intensities. Plotting this series makes it simpler to follow how the electric field affects the intensity of the luciferase solution.

Figure 4.16 shows a plot of average intensities from an early experiment. In this experiment, a high electric field is applied and removed by manually enabling and disabling the output of a function generator. The function generator was set to create a 100 kHz sine wave at 10 Vpp. It was later discovered that it is also important to measure the actual voltage across the die, as small differences in the device create enough of an impedance mismatch to noticeably affect the field's magnitude.

Examining this graph shows that when the electric field is turned on, the average intensity falls sharply and remains at this lower level until the field is turned off. When the field is turned off, the average intensity increases again. In this graph, both the higher intensity (function generator off) and the lower intensity (function generator on) seem to follow the half-life curve.

After reliably reproducing the results in Figure 4.16, we automated control of the function generator to produce consistent on/off periods. Figure 4.17 shows the data from one of these experiments. The function generator is set to 9 Vpp at 100 kHz. The voltage across the die, measured by oscilloscope, is 15.02 Vpp, giving an electric field strength of

---

[1] This range of wavelengths was chosen because it encompasses the entire spectrum emitted by the luciferase solution.

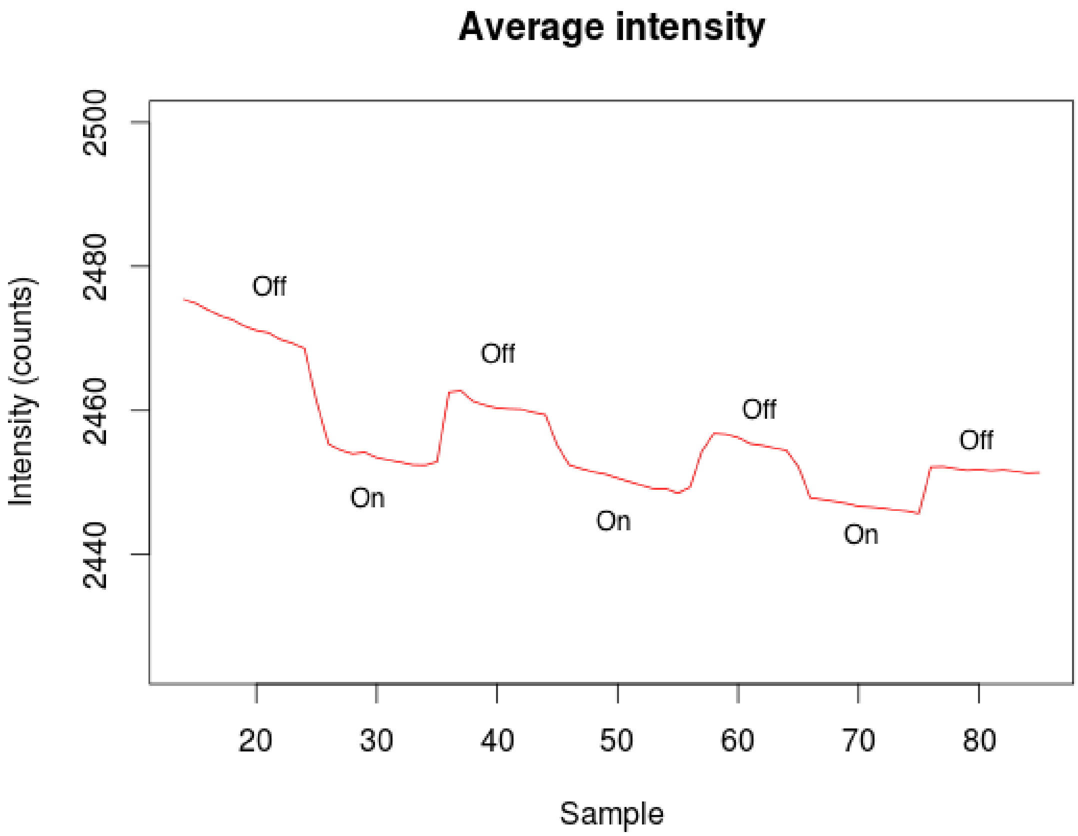

Figure 4.16: This graph shows how the electric field affects the average intensity of the light emitted by the luciferase solution. Each time the field is enabled, the intensity drops. When the field is disabled, the intensity increases. Note how the decay in intensity when the field is off and on follows the half-life decay expected from experiments in Section 3.1. In this test, the function generator creating the electric field is set to a sine wave with 10 Vpp at 100 kHz. The die being tested has a gap of 20 µm. An oscilloscope was not used to check the actual voltage across the die during this test.

approximately 0.75 MV/m. Each period consists of 5 "on" and 5 "off" samples. Each sample is taken with a spectrometer set to have a 20 second integration time.

Like the early results, enabling the electric field drops the intensity and subsequently disabling the field increases the intensity. The "off" samples follow the expected half-life decay. The "on" samples do not seem to be following the half-life decay seen with the "on" samples in Figure 4.16. However, these "on" samples pull the intensity within three standard deviations of the noise floor. As such, the lack of an obvious exponential decay with the "on"

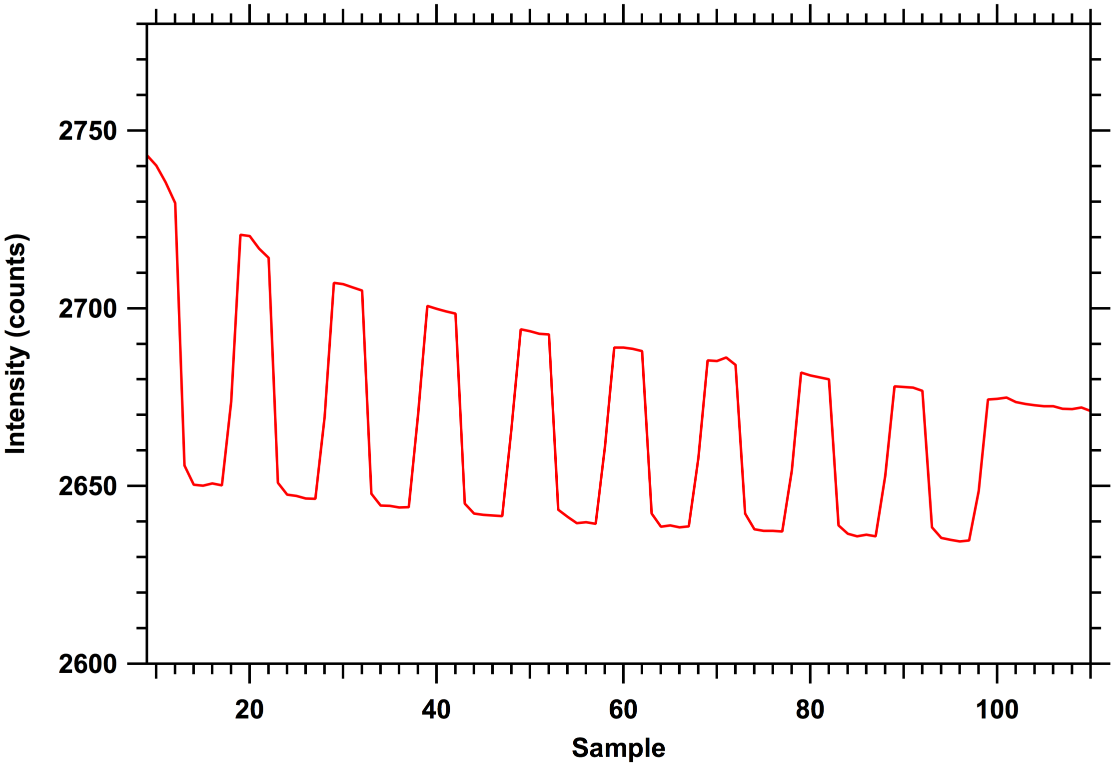

Figure 4.17: This graph shows how the electric field affects the average intensity of the light emitted by the luciferase solution. Each time the field is enabled, the intensity drops. When the field is disabled, the intensity increases. Note how the decay in intensity when the field is off follows the half-life decay expected from experiments in Section 3.1. In this test, the function generator creating the electric field is set to a sine wave with 9 Vpp at 100 kHz. The die being tested has a gap of 20 µm. The voltage across the die was measured at 15.02 Vpp using an oscilloscope. This gives an electric field of approximately 0.75 MV.

samples may indicate that the spectrometer is not correctly detecting light levels so close to the noise floor. Regardless, we are consistently able to reproduce this drop in intensity by applying a high electric field across luciferase.

Chapter 5

Conclusion

This repeatable ability to affect emitted light intensity by applying an electric field is promising. The fact that it is not accompanied by a shift in wavelength suggests that the effect is not a product of heating. Additionally, the intensity decreases when the electric field is applied. The heat sink attached to the device is held at 22 °C. If the electric field increased the temperature of the luciferase, this should result in an increase of intensity. Since the intensity instead *decreased*, this suggests that the shift in intensity had another cause. We believe that this drop in intensity represents a decreased luciferase activity due to topological distortions caused by the electric field.

While it seems plausible that this decrease in activity could be caused by the electric field distorting the secondary and/or tertiary structures of the protein, further work is needed to ensure that this is the case. One avenue that could validate this is to model the chemical reaction to see how the reaction mechanism is altered when a high electric field is applied and to see how this results in a decrease in luminescence.

It would also be useful to test the device using a range of electric field strengths. In one test not shown, a graph of the average intensity seemed to indicate that there is threshold to the electric field strength below which luciferase activity is unaffected. Characterizing at what field strength this affect begins would provide useful information. Additionally, it could help verify any modeling results.

A third area that would be useful to explore is how the frequency of the electric field affects this process. It is expected that this process will only work between 1 kHz and 10 MHz, but that leaves a wide range of possible frequencies.

Further exploration of this phenomena will help us understand how high electric fields can interfere with protein function. As our understanding of the relationship between the two increases, it seems likely that, using existing rDNA processes, it should be possible to design and produce proteins which can be switched using electric fields. In this way, protein functions could be targeted to activate at a particular location and time.

Bibliography

[1] T. O. Baldwin, "Firefly luciferase: the structure is known, but the mystery remains." *Structure*, vol. 4, no. 3, pp. 223–8, Mar. 1996. [Online]. Available: http://www.ncbi.nlm.nih.gov/pubmed/8805542http://www.sciencedirect.com/science/article/pii/S0969212696000263 vii, 1, 6, 7, 8

[2] H. Wan, S. Sun, X. Hu, and Y. Xia, "Nonthermal effect of microwave irradiation in nonaqueous enzymatic esterification." *Applied biochemistry and biotechnology*, vol. 166, no. 6, pp. 1454–62, Mar. 2012. [Online]. Available: http://www.ncbi.nlm.nih.gov/pubmed/22262019 1

[3] G. Y. Solomentsev, N. J. English, and D. a. Mooney, "Effects of external electromagnetic fields on the conformational sampling of a short alanine peptide." *Journal of computational chemistry*, vol. 33, no. 9, pp. 917–23, Apr. 2012. [Online]. Available: http://www.ncbi.nlm.nih.gov/pubmed/22328143 1

[4] W. Zhao and R. Yang, "Pulsed Electric Field Induced Aggregation of Food Proteins: Ovalbumin and Bovine Serum Albumin," *Food and Bioprocess Technology*, vol. 5, no. 5, pp. 1706–1714, Nov. 2010. [Online]. Available: http://www.springerlink.com/index/10.1007/s11947-010-0464-8 1

[5] W. Zhao, R. Yang, X. Hua, W. Zhang, Y. Tang, and T. Chen, "Inactivation of Polyphenoloxidase of Pear by Pulsed Electric Fields," *International Journal of Food Engineering*, vol. 6, no. 3, Jan. 2010. [Online]. Available: http://www.degruyter.com/view/j/ijfe.2010.6.3/ijfe.2010.6.3.1853/ijfe.2010.6.3.1853.xml 1

[6] W. Zhao and R. Yang, "Experimental study on conformational changes of lysozyme in solution induced by pulsed electric field and thermal stresses." *The journal of physical chemistry. B*, vol. 114, no. 1, pp. 503–10, Jan. 2010. [Online]. Available: http://www.ncbi.nlm.nih.gov/pubmed/19899791 1

[7] N. J. English, G. Y. Solomentsev, and P. O'Brien, "Nonequilibrium molecular dynamics study of electric and low-frequency microwave fields on hen egg white lysozyme." *The Journal of chemical physics*, vol. 131, no. 3, p. 035106, July 2009. [Online]. Available: http://www.ncbi.nlm.nih.gov/pubmed/19624238 1

[8] A. Budi, F. S. Legge, H. Treutlein, and I. Yarovsky, "Electric field effects on insulin chain-B conformation." *The journal of physical chemistry. B*, vol. 109, no. 47, pp. 22 641–8, Dec. 2005. [Online]. Available: http://www.ncbi.nlm.nih.gov/pubmed/16853947 1

[9] S. Toepfl, a. Mathys, V. Heinz, and D. Knorr, "Review: Potential of High Hydrostatic Pressure and Pulsed Electric Fields for Energy Efficient and Environmentally Friendly Food Processing," *Food Reviews International*, vol. 22, no. 4, pp. 405–423, Dec. 2006. [Online]. Available: http://www.tandfonline.com/doi/abs/10.1080/87559120600865164 1

[10] S.-c. Tu, "Isolation and Properties of Bacterial Luciferase-Oxygenated Flavin Intermediate Complexed with Long-chain Alcoholst," pp. 5940–5945, 1979. 2

[11] H. Zhao, T. Doyle, O. Coquoz, F. Kalish, B. Rice, and C. Contag, "Emission spectra of bioluminescent reporters and interaction with mammalian tissue determine the sensitivity of detection in vivo," *Journal of Biomedical Optics*, vol. 10, no. 4, 2005. 2, 4, 12

[12] R. Murray, H. Harper, D. Granner, P. Mayes, and V. Rodwell, *Harper's Illustrated Biochemistry*, 27th ed. New York: McGraw-Hill, 2006. 3

[13] J. Antosiewicz, "Computation of the dipole moments of proteins." *Biophysical journal*, vol. 69, no. 4, pp. 1344–54, Oct. 1995. [Online]. Available: http://www.pubmedcentral.nih.gov/articlerender.fcgi?artid=1236364&tool=pmcentrez&rendertype=abstract 3

[14] J. Antosiewicz and D. Porschke, "The nature of protein dipole moments: experimental and calculated permanent dipole of alpha-chymotrypsin." *Biochemistry*, vol. 28, no. 26, pp. 10 072–8, Dec. 1989. [Online]. Available: http://www.ncbi.nlm.nih.gov/pubmed/2620062 3

[15] G. von Heijne, "Control of topology and mode of assembly of a polytopic membrane protein by positively charged residues." *Nature*, vol. 341, no. 6241, pp. 456–458, 1989. [Online]. Available: http://europepmc.org/abstract/MED/2677744 3

[16] D. Kiefer, X. Hu, R. Dalbey, and a. Kuhn, "Negatively charged amino acid residues play an active role in orienting the Sec-independent Pf3 coat protein in the Escherichia coli inner membrane." *The EMBO journal*, vol. 16, no. 9, pp. 2197–204, May 1997. [Online]. Available: http://www.pubmedcentral.nih.gov/articlerender.fcgi?artid=1169822&tool=pmcentrez&rendertype=abstract 3

[17] B. Rost, P. Fariselli, and R. Casadio, "Topology prediction for helical transmembrane proteins at 86% accuracy." *Protein science : a publication of the Protein Society*, vol. 5, no. 8, pp. 1704–18, Aug. 1996. [Online]. Available: http://www.pubmedcentral.nih.gov/articlerender.fcgi?artid=2143485&tool=pmcentrez&rendertype=abstract 3

[18] C. Rutz, W. Rosenthal, and R. Schülein, "A Single Negatively Charged Residue Affects the Orientation of a Membrane Protein in the Inner Membrane of Escherichia coli Only When It Is Located Adjacent to a Transmembrane Domain," *Journal of Biological Chemistry*, vol. 274, no. 47, pp. 33 757–33 763, Nov. 1999. [Online]. Available: http://www.jbc.org/cgi/doi/10.1074/jbc.274.47.33757 3

[19] R. J. Naumann, *Introduction to the Physics and Chemistry of Materials.* CRC Press, 2009. 4

[20] F. W. Sears, M. W. Zemansky, and H. D. Young, *College Physics.* Addison-Wesley Pub. Co., 1985. 5

[21] K. V. Wood, Y. A. Lam, H. H. Seliger, and W. D. McElroy, "Complementary DNA coding click beetle luciferases can elicit bioluminescence of different colors." *Science (New York, N.Y.)*, vol. 244, no. 4905, pp. 700–702, May 1989. [Online]. Available: http://europepmc.org/abstract/MED/2655091 8

[22] Promega, "ONE-Glo Luciferase Assay System," p. 19, 2012. [Online]. Available: http://www.promega.com/~/media/Files/Resources/Protocols/TechnicalManuals/0/ONE-GloLuciferaseAssaySystemProtocol.pdf 11, 12, 14

[23] J. P. Barber, "Fabrication of Hollow Optical Waveguides on Planar Substrates," Ph.D. dissertation, 2006. 20

[24] M. Wu, "Micromachining for optical and optoelectronic systems," *Proceedings of the IEEE*, vol. 85, no. 11, pp. 1833–1856, 1997. [Online]. Available: http://ieeexplore.ieee.org/lpdocs/epic03/wrapper.htm?arnumber=649660 20

[25] B. E. A. Saleh and M. C. Teich, *Fundamentals of Photonics*, ser. Wiley Series in Pure and Applied Optics. John Wiley & Sons, 2007. [Online]. Available: http://books.google.com/books?id=Ve8eAQAAIAAJ 41

[26] C. Palmer and E. Loewen, *Diffraction Grating Handbook*, 6th ed. Rochester: Newport Corporation, 2005. [Online]. Available: http://gratings.newport.com/library/handbook/handbook.asp 41, 42

[27] J. M. Lerner, "Imaging Spectrometer Fundamentals for Researchers in the Biosciences A Tutorial," *Cytometry, Part A*, vol. 69A, pp. 712–734, 2006. [Online]. Available: http://www.lightforminc.com/ImagingSpectrometerFundamentals.pdf 42

Appendix A

Spectral Resolution vs Light Collection in Diffraction Grating Optical Spectrometers

A.1 Introduction

Optical spectrometers are used to map the distribution of wavelengths in the UV, visible, and NIR ranges. They are commonly used to measure absorbance, transmission, and emission characteristics.

This paper discusses the physical optics behind diffraction grating spectrometers in an attempt to explain the trade-off between spectral resolution and light collection. In research that uses nonstandard collection apertures, this understanding may help with interpreting how an observed spectrum relates to the actual spectrum of the source. This may be particularly applicable when working in low-light settings.

A.2 Diffraction and Spectrometry

Spectrometers require a dispersive element to separate wavelengths into a measurable spectrum. Prisms and diffraction gratings can both act as dispersive elements, but commercial spectrometers tend to make use of diffraction gratings. Figure A.1 shows a diagram of a diffraction grating dispersing light.

A simple spectrometer is shown in Figure A.2. Light from the source enters through a slit. It is then collimated before reaching the diffraction grating. The diffraction grating is angled so one of the diffraction orders covers an optical sensor.

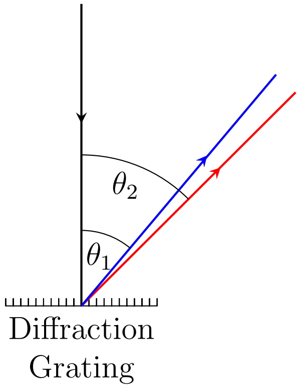

Figure A.1: Light incident on a diffraction grating is diffracted at different angles, dependent on wavelength.

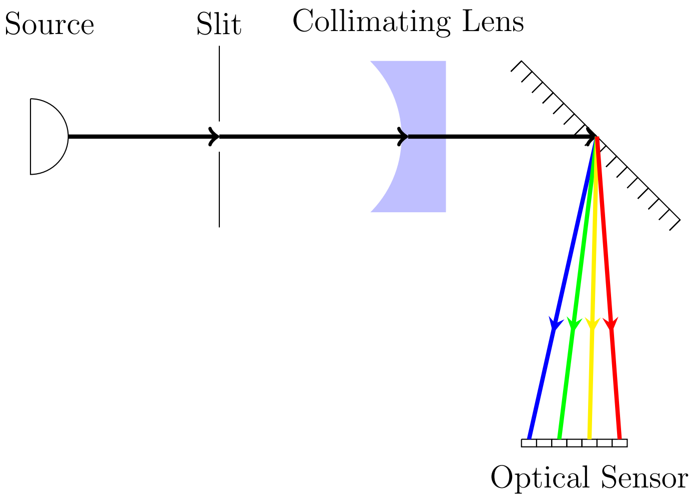

Figure A.2: Diagram of the optical components in a diffraction grating spectrometer.

Light incident on a diffraction grating is dispersed into multiple orders. The equations that follow show the relationship between order number, m, wavelength, λ, groove separation, d, and the angles of light incident on the grating, θ_i, and dispersed by the grating, θ_m[25]

$$m\lambda = d\left(\sin\theta_m + \sin\theta_i\right), \tag{A.1}$$

$$\theta_m = \arcsin\left(\frac{m\lambda}{d} - \sin\theta_i\right). \tag{A.2}$$

By rearranging Equation A.1 in terms of the angle of the diffracted ray, we see that higher diffraction orders result in greater dispersion while the zeroth order produces no dispersion. This increase in dispersion comes at the cost of decreased intensity.

A.3 Spectral Resolution vs. Optical Power

In general, an increase in spectral resolution results in a decrease in photon collection and vice versa. This section examines that trade-off by examining spectral resolution and optical power under ideal circumstances and then by demonstrating this trade-off experimentally.

A.3.1 Spectral Resolution

In this context, spectral resolution is a measure of how well the spectrometer is able to distinguish between two adjacent wavelengths. It is convenient to measure resolution in terms of $\Delta\lambda$, the limit of resolution, the difference between two wavelengths of equal intensity that can be distinguished [26]. Commercially available spectrometers typically have spectral resolutions on the order of 1 nm or 0.1 nm with high resolution spectrometers on the order of 0.01 nm.

Before discussing how components of a spectrometer contribute to the spectrometer resolution, it is important to note that the signal observed is a function of the spectrometer resolution and the source spectrum. More precisely, the observed spectrum is a convolution of the source spectrum and the resolution of the spectrometer [27]

$$S_{\text{observed}}(\lambda) = S_{\text{source}}(\lambda) * R_{\text{spectral}}(\lambda). \tag{A.3}$$

If the source spectrum is much more narrow than the resolution, the observed spectrum becomes a measure of the resolution of the spectrometer (centered on the source spectrum)

$$S_{\text{source}}(\lambda) \ll R_{\text{spectral}}(\lambda), \tag{A.4}$$
$$S_{\text{observed}}(\lambda) \approx R_{\text{spectral}}(\lambda). \tag{A.5}$$

Similarly, if the spectrometer resolution is significantly finer than the linewidth of the source, the spectrum observed is approximately the spectrum of the signal

$$S_{\text{source}}(\lambda) \gg R_{\text{spectral}}(\lambda), \tag{A.6}$$
$$S_{\text{observed}}(\lambda) \approx S_{\text{source}}(\lambda). \tag{A.7}$$

Therefore, as might be expected, the resolution of the spectrometer should be significantly finer than the features in the source spectrum.

Three components that significantly affect the resolution of a spectrometer are the resolving power of the diffraction grating, the width and number of pixels in the optical sensor, and the width of the entrance slit. Starting with resolving power, we will examine the effect of each component on spectral resolution.

Resolving power is a measure of how well a grating separates adjacent wavelengths [27, 26]. Mathematically, this can be expressed as

$$R = \frac{\lambda}{\Delta\lambda}, \tag{A.8}$$

where λ is the central wavelength and $\Delta\lambda$ is the limit of resolution.

The resolving power for an ideal, planar grating is

$$R = \left|mN\right|, \tag{A.9}$$

where N is the number of illuminated grooves and m is the diffraction order [26].

Solving Equation A.1 for the diffraction order, m, and substituting it in to Equation A.9 gives

$$R = \left|\frac{Nd\left(\sin\theta_m + \sin\theta_i\right)}{\lambda}\right|, \tag{A.10}$$

where θ_i is the angle of incidence and θ_m is the diffraction angle of a given diffraction order. Assuming a uniform groove spacing, d, we can replace Nd with the width of the grating, W_d, we have

$$R = \left|\frac{W_d\left(\sin\theta_m + \sin\theta_i\right)}{\lambda}\right|. \tag{A.11}$$

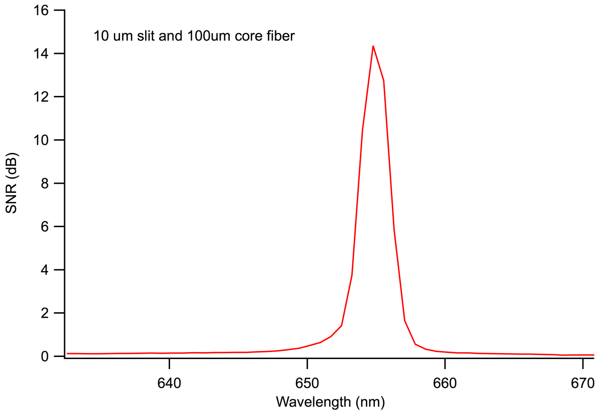

(a) 100 µm core fiber attached to a 10 µm slit.

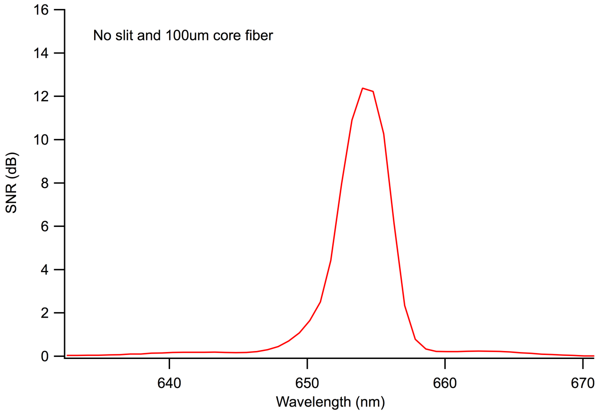

(b) 100 µm core fiber without slit (1000 µm aperture at the spectrometer).

Figure A.3: Comparison of a 100 µm fiber with and without a slit collecting light from a red laser pointer. Without the slit, the spectral resolution becomes slightly coarser.

Finally, since $|\sin\theta_m + \sin\theta_i|$ must be less than 2, the maximum resolving power for an ideal, planar grating can be given as a function of width and wavelength

$$R_{max} = \frac{2W_d}{\lambda}. \tag{A.12}$$

Equating this derived maximum resolving power with Equation A.8, we can find the lower bound of the limit of resolution

$$\Delta\lambda = \frac{\lambda^2}{2W_d}. \tag{A.13}$$

The next limiting factor to consider is the width and number of pixels in the optical sensor. Assuming an infinitesimally thin beam incident on the diffraction grating, the resolution will be limited by the dispersion of the grating and the pixel width and number of

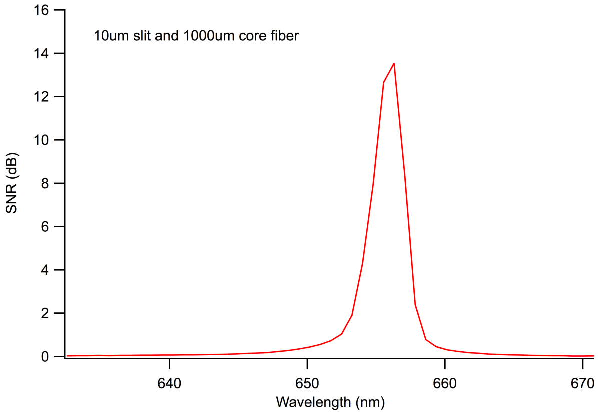

(a) 1000 µm core fiber attached to a 10 µm slit.

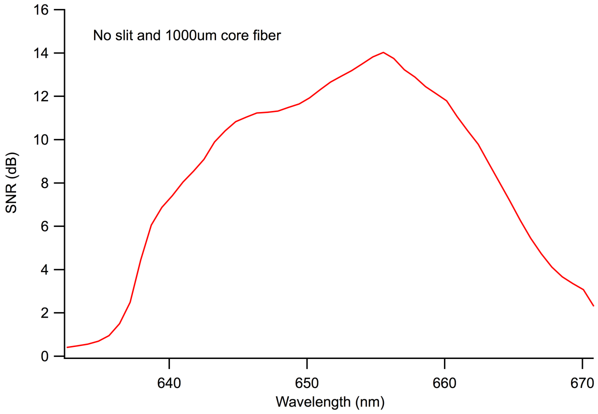

(b) 1000 µm core fiber without slit (1000 µm aperture at the spectrometer).

Figure A.4: Comparison of a 1000 µm fiber with and without a slit collecting light from a red laser pointer. Without the slit, the spectral resolution is much coarser.

pixels on the optical sensor

$$\Delta\lambda_{\text{pixel,min}} = \frac{\Delta\lambda_{\text{grating}}}{n \times W_p}. \tag{A.14}$$

Here $\Delta\lambda_{\text{grating}}$ is the spectral range of the grating, n is the number of pixels, and W_p is the width of a single pixel.

Assuming that the beam incident on the diffraction grating has a beamwidth equal to the width of the entrance slit, W_s, it follows that the pixel resolution of a spectrometer can be expressed as

$$\Delta\lambda_{\text{pixel}} = \frac{\Delta\lambda_{\text{grating}}}{n \times W_p} \times W_s. \tag{A.15}$$

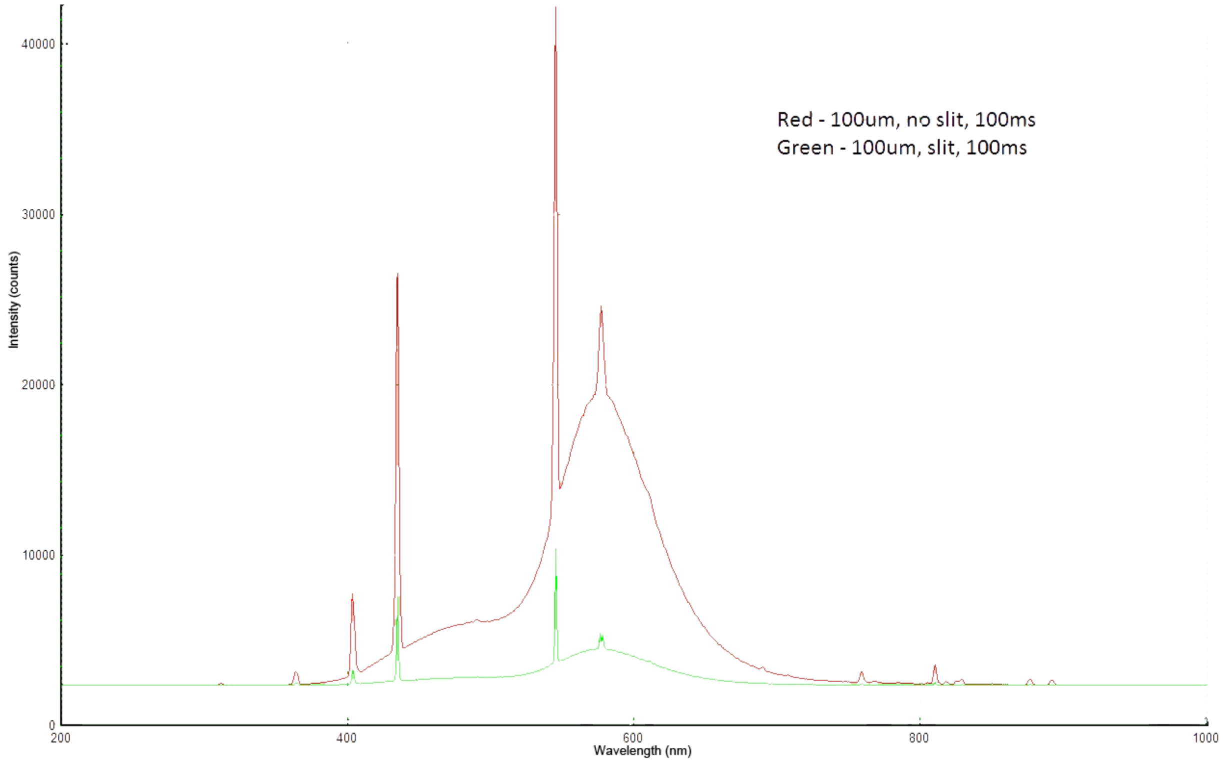

Figure A.5: A 100 µm core with and without the 10 µm slit (without slit, the entrance aperture is 1000 µm). The light source is a commercial overhead fluorescent light. This demonstrates how the slit dramatically decreases the number of photons collected by the spectrometer.

A.3.2 Optical Power

The intensity of light diffracted off a grating decreases with higher diffraction orders. The exact intensity illuminating the optical sensor is dependent on the properties of the grating and which order is measured. However, it is safe to assume the upper limit of intensity is the intensity that passes through the entrance slit, I_s. Assuming the source is able to evenly illuminate a spot much larger than the entrance slit, I_s will not change with slit width.

The optical power incident on the sensor therefore has an upper limit of

$$P = I_s \times A, \tag{A.16}$$

where A is the area of the entrance slit. It follows that optical power increases linearly with slit area.

A.3.3 Experimental Results

Two experiments were performed to examine how spectral resolution and observed power depend on aperture size. In both, data was gathered using an Ocean Optics QE6500.

Table A.1: Vendor provided resolution compared with measured resolution at different aperture sizes.

	Vendor Provided	Experimental
10 µm	1.58 nm	2 nm
100 µm	3.38 nm	3.8 nm
1000 µm	None given	15.3 nm

To test resolution, light from a red laser was coupled into the spectrometer through three different aperture sizes. Aperture size was varied by using or not using an entrance slit (10 µm aperture with the slit, 1000 µm aperture without) and by switching between 100 µm core fiber and 1000 µm core fiber. The laser used was a Wilcom F6230A VFL with the following vendor specifications:

- Center wavelength – 650 ± 20 nm
- Output power – 0.4 mW to 1 mW
- Spectral width – under 5 nm.

The results can be seen in Figures A.3 and A.4. These figures show intensity[1] the spectrum of a red laser pointer using various aperture sizes (W_s). The graphs have the following aperture widths:

- $W_s = 10$ µm (Figures A.3a and A.4a)
- $W_s = 100$ µm (Figure A.3b)
- $W_s = 1000$ µm (Figure A.4b).

As expected, an increase in the aperture size increases the FWHM linewidth increases.

For convenience, vendor provided resolutions for a given aperture are compared to the experimental results in Table A.1.

To test photon collection, light from a commercial, fluorescent light fixture coupled into the spectrometer. Figure A.5 demonstrates the difference in intensity between a 10 µm aperture and a 100 µm aperture. This figure shows intensity (in photon counts) as a function of wavelength. The 10 µm reduces the photon count by 75% compared to the 100 µm aperture. Comparing this decrease in intensity with the potential resolution gain is an excellent example of the trade-off between spectral resolution and light collection.

A.4 Conclusion

Understanding the limitations of data-collection hardware helps both with interpreting data and designing future experiments. With spectroscopy, understanding the relationship between spectral resolution and light collection can be especially useful in designing

---

[1] Intensity is normalized by noise to give SNR.

experiments. For example, when analyzing the spectrum of a low-light source, understanding this trade-off and Equation A.3 helps the researcher decide which aperture size is necessary to collect accurate data on the source. Similarly, when analyzing a source with a narrow linewidth, the researcher could do a back-of-the-envelope calculation to approximate how much optical power, and whether the experiment is feasible. By understanding these limitations, the researcher can improve the number of experiments yielding useful data.

Appendix B

Fabrication Processes

B.1 Photolithography for Patterning Electrodes

1. Dehydration bake at 150 °C for 5 minutes.
2. Dispense about 2 or 3 drops of HMDS on the wafer.
3. Spin at 4000 rpm for 30 s and then ramp up to 6000 rpm for 2 s.
4. Dispense AZ3330 on the wafer.
5. Spin at 4000 rpm for 30 s and then ramp up to 6000 rpm for 2 s.
6. Bake at 90 °C for 1 min.
7. Expose for 10 s with a 50 µm alignment gap using the south aligner.
8. Develop in 300MIF developer for 60 s.
9. Hard Bake at 110 °C for 1 min.

This process should give a photoresist height of approximately 3 µm.

B.2 Etching Electrodes

1. Heat the aluminum etchant to 50 °C.
2. Place the wafer in a Teflon wafer holder.
3. Place the teflon wafer holder into the aluminum etchant.
4. Etch for approximately 50 s.
5. Rinse with DI water for 30 s on both sides.
6. Dry with N_2 gas.
7. Rinse with IPA and acetone to remove the photoresist.

B.3 Fluid Channel Fabrication

1. Dehydration bake at 150 °C for 5 minutes.
2. Plasma descum at 100 W for 30 s.
3. Dispense HMDS and SU8-2025.
4. Spin at 500 rpm for 6 s, and then at 4000 rpm for 30 s and then ramp up to 6000 rpm for 2 s.
5. Bake at 65 °C for 3 minutes.
6. Bake at 95 °C for 5 minutes.
7. Expose for 30 s, with a 130 µm alignment gap using the south aligner.
8. Bake at 95 °C for 5 minutes.
9. Develop in SU8 developer for 80 s.

The photoresist should be approximately 20 µm tall. When the slide is attached, this will give us a 20 µm deep channel.

B.4 Attach ITO Cover Slip

1. Place a ITO slide on the sample.
2. Put the sample in the aluminum clamp.
3. Place a piece of aluminum foil and PDMS on top of the slide[1].
4. Tighten the clamp.
5. Bake at 225 °C for 5 minutes.
6. Test the channel surface to ensure that it is hydrophobic.

---

[1] The PDMS helps distribute the pressure more evenly. The aluminum foil helps in removing the PDMS afterwards.